A High-Frequency Ground-Penetrating Radar Study of The Randolph Kimberlites, Riley County, Kansas

Kansas Geological Survey Open File Report 95-59

Joseph M. Kruger[1], Alex Martinez[1], Pieter Berendsen[1],
Mike L. Shoemaker[2],

[1]Kansas Geological Survey, Lawrence, KS
[2]University of Missouri-Rolla, Rolla, MO

Kansas Geological Survey
Open-file Report

Disclaimer

The Kansas Geological Survey does not guarantee this document to be free from errors or inaccuracies and disclaims any responsibility or liability for interpretations based on data used in the production of this document or decisions based thereon. This report is intended to make results of research available at the earliest possible date, but is not intended to constitute final or formal publication.

INTRODUCTION

A pilot study to determine the usefulness of high-frequency ground-penetrating radar (GPR) methods in delineating the geometry of kimberlites was undertaken in the Spring of 1995. High-frequency ground-penetrating radar methods are capable of resolving shallow subsurface features in great detail in a manner analogous to reflection seismic data. This has the potential of identifying the margins of a kimberlite intrusion in the shallow subsurface where outcrop information is limited or nonexistent.

This report focuses on the Randolph 1 and Randolph 2 kimberlite intrusions in Riley County, Kansas (Fig. 1). Six 45.7 m (150 ft) long GPR profiles were gathered at the Randolph 1 study site (Fig. 2), and five, 38.1-45.7 m (125-150 ft) long GPR profiles were gathered at the Randolph 2 study site (Fig. 3). Acquisition of the data was aimed at imaging features associated with the margins of the kimberlite intrusions such as the contact between the kimberlites and host rock, and other indirect indicators such as folding or brecciation of surrounding units as the intrusions are approached. The Randolph 1 and 2 study sites were chosen because of ease of access, relatively thin soil cover, limestone host rock near the surface, and exposures of the kimberlite intrusions. Results from this experiment suggest that high-frequency GPR methods could be used to delineate the near-surface extent of a kimberlite intrusion (and possibly other forceful intrusions), depending on the surrounding host rock, soil type, and soil thickness.

GEOLOGIC SETTING

At least ten kimberlites are known to intrude rocks of the lower Permian Chase Group in Riley County. Five are exposed at the surface, while the rest are buried under a thin soil cover. Cretaceous rocks of unknown thickness probably covered the area and have been eroded since that time. During the course of exploration activities well-bedded tuff was exposed in a trench at Winkler "crater", indicating that the kimberlite magma reached the surface in at least that location (Berendsen et al, 1985). Based upon a study of sets of joint patterns present in the kimberlites and Lower Permian and early Late Cretaceous rocks, a maximum age of emplacement of 100 ± 20 m.y. may be inferred from geologic evidence (Brookins and Naeser, 1971). K-Ar dates on chloritized biotite and phlogopite range from 112 to 380 m.y. (Brookins and Naeser, 1971). Age dates on similar alkaline intrusions in the midcontinent area are approximately 90 m.y. Thus, an age of around 100 m.y. for the intrusions seems reasonable. The kimberlites are pervasively carbonatized and fluid inclusion homogenization temperatures of late-stage carbonate veins yield relatively low temperatures in the 240-250^{o} C range (Mansker et al, 1987).

Structurally, the kimberlites are roughly aligned with a prominent north-northeast-trending structure known as the Abilene Anticline (Jewett, 1951) (Fig. 1). Later studies indicate that the Abilene Anticline is a major horst, bounded by deep-seated faults associated with the 1,100 m.y.-old Midcontinent Rift system (Berendsen and Blair, 1992). More detailed structural analyses indicate that the kimberlites tend to occur at the intersection of north-northeast- and northwest-trending faults that coincide with the main structural trend in eastern Kansas and surrounding areas.

The Randolph 1 kimberlite (Fig. 2) forms a circular knoll about 3 m (10 ft) high and 61 m (200 ft) in diameter. The Towanda Limestone Member of the Doyle Shale is bent up at the contact with the kimberlite, but flat lying within a meter of the country rock (Byrne et al, 1956).

The Randolph 2 kimberlite (Fig. 3) forms a nearly circular knoll about 15 m (50 ft) in diameter on an eastward-sloping hill of the Fort Riley Limestone Member of the Barneston Limestone (Brookins, 1970a). Mapping and drilling suggest that the Randolph 2 kimberlite is an elliptical intrusion with a mushroom-shaped cap above a narrow east-southeast-dipping feeder pipe (Brookins, 1970a) (Fig. 4). Beds of the Fort Riley Limestone dip away from the intrusion.

GPR METHODS, DATA COLLECTION, AND PROCESSING

Methods

Ground-penetrating radar (GPR) is a high-resolution near-surface geophysical technique using antennas to send electromagnetic pulses into the ground in order to image the subsurface via returned reflection energy. Similar to seismic reflection methods, where reflections are caused by boundaries associated with acoustical impedance contrasts, GPR reflections are caused by the electromagnetic waves encountering media of different electrical properties - namely boundaries consisting of a contrast in the dielectric constant of the material above and below the boundary. Values for dielectric constants (K) range from 1 for air, 81 for water, 3-5 for dry sand, 4-8 for limestone, 5-13 for shale, 5-40 for clay (Davis and Annan, 1989), 6.6 for serpentine, and 8.6 for peridotite (Telford et al., 1976). Dielectric constant values affect the velocity of electromagnetic waves through a material, and are related to velocity by:

$$\text{velocity} = \frac{c}{\sqrt{K\mu_r}}$$

where $c = 3 \times 10^8$ m/s (speed of light in a vacuum), and μ_r is the relative magnetic permeability of the material. In non-magnetic materials $\mu_r=1$, which reduces the above equation to:

$$\text{velocity} = \frac{c}{\sqrt{K}}$$

Using the relationship given above, one-way velocities for materials range from 0.3 m/ns (meters/nanosecond) for air, 0.033 m/ns for water, 0.134-0.173 m/ns for dry sand, 0.11-0.15 m/ns for limestone, 0.077-0.134 m/ns for shale, 0.047-0.134 m/ns for clay, 0.12 m/ns for serpentine, and 0.10 m/ns for peridotite. The presence of magnetite and ilmenite in the kimberlites might decrease the velocity of electromagnetic waves passing through them because of maximum relative magnetic permeabilities greater than 1 (magnetite=5, ilmenite=1.55; Telford et al., 1976). However, due to the low bulk percentage of these magnetic minerals in the kimberlites, the effect should not be that great. Differences in dielectric constant across boundaries also determine the strength of reflections from those boundaries. According to Davis and Annan (1989) the reflection coefficient (R) at a half-space for a normal incident signal is determined by:

$$R = \frac{\sqrt{K_1} - \sqrt{K_2}}{\sqrt{K_1} + \sqrt{K_2}}$$

where layer 1 is above layer 2. Another important electrical property is the conductivity of the medium. The higher the conductivity, the more the signal attenuates, causing a shallower penetration depth for usable information (Davis and Annan, 1989).

Antenna frequencies typically range from 10 MHz to 1000 MHz (a 500 MHz antenna was used in this study), and imaging resolution is proportional to antenna frequency, while penetration depth is inversely proportional to antenna frequency (the greater the antenna frequency, the less penetration but greater detail). Vertical resolution varies from 1-1.5 m (3-5 ft) for low-frequency antennas (10-100 MHz), to 0.02-0.3 m (1-12 in) for high-frequency antennas (500-1000 MHz) for most materials (Davis and Annan, 1989).

GPR profiles have a similar appearance to seismic profiles, and usually are represented as common depth point (cdp) data, with amplitude variations representing differences in reflection energy. As with seismic data, vertical scales are in time (or depth if the data have been depth migrated), while lateral scales are in distance. However, the scales differ by several orders of magnitude; GPR records have lengths measured in nanoseconds (1×10^{-9} s), compared to milliseconds (1×10^{-3} s) in seismic records. Also, the distances between cdps in GPR profiles are usually much smaller than seismic profiles (an average GPR cdp spacing of 3 cm in this study, versus standard, near-surface seismic reflection cdp spacing of 0.3-1.5 m for high-resolution profiles).

Equipment & Data Collection

Preparation of the study site included clearing the antenna path of obstructions, flagging stations along the antenna path, and collecting relative elevation information for the stations. The clearing of material such as small rocks and clumps of grass from the antenna pathway greatly enhanced the coupling of the antenna with the ground during the data collection process. In addition, by clearing the pathway of obstructions, lateral movement of the antenna stayed at a relatively consistent velocity and ensured even cdp coverage. Relatively tall grass at the Randolph 1 site was cut along the antenna path before acquiring the data. Station flagging at a 1.5 m (5 ft) interval served several purposes. It assisted in retaining the same antenna pathway for each of the various scan lengths (record lengths). It also allowed the GPR data to be correlated to specific ground locations, and ensured some lateral control during data collection. The collection of relative elevation information from stations every 7.6 m (25 ft) allowed the data to be corrected for elevation differences during processing. These corrections immensely aided the interpretation of reflection information and correlation with outcrop information. Elevations were obtained using a level and rod, and are accurate to within $\pm$ 3 cm. Six parallel northwest-trending GPR profiles, each 45.7 m (150 ft) long, were acquired along the northwest margin of the Randolph 1 kimberlite (Fig. 2). Acquisition was limited to this part of the kimberlite because of a fence and thick soil (Qal) elsewhere (Fig. 2). Five lines were acquired in a star-burst pattern at the Randolph 2 site with the start of each line located near the center of the kimberlite (Fig. 3). Line locations at this site were limited by trees. Three of the lines are 45.7 m (150 ft) long while the other two are 38.1 m (125 ft) long (Fig. 3). Both the elevation data and field observations of the kimberlite outcrop suggest that the start of each line (station 0) is close to a previously drilled borehole (power auger drill site #2 on Figures 3 and 4) (Brookins, 1970a). Because of this, station 0 was assumed to be located at drill site #2 for the purposes of geologic correlation in this report.

The equipment used for the study was a GSSI SIR System-8 GPR unit, with a DT6000A tape unit and 500-MHz dominant-frequency monostatic antenna (transmitting and receiving antenna the same). Use of a monostatic system allowed for rapid acquisition but precluded measurement of any velocity information. Because of this, depth conversions were not performed. A scan length of 80 ns was recorded at a rate of 12.8 scans/second as the antenna was pulled along the line. The tape unit recorded coherent system noise beginning at approximately 40 ns on each trace. This noise masked most of the reflection information below 40 ns, greatly reducing the signal-to-noise ratio at the longer scan times. Digital filtering of the data removed some, but not all, of the noise. A short marker-pulse was recorded whenever passing a flagged station (every 1.5 m; 5 ft), and a double pulse was recorded at every fifth flag (every 7.6 m; 25 ft). This enhanced control over how fast the antenna was pulled along the ground, and allowed correlation between data and outcrop.

Data Processing

The data were downloaded from the DT6000A tape unit and converted from RADAN format into 4-byte SEGY format before importation into Seismic Unix (SU) on a workstation. Once within SU, the data were time- and distance-scaled by a factor of $1x10^6$ for viewing and processing purposes. The 80 ns scan data had 512 samples per trace, a sample interval of 0.156 ns, and a lateral distance (cdp trace spacing) of approximately 3 cm per trace.

The GPR data were treated as stacked seismic reflection data within SU, opening up the possibility of post-stack digital processing. Front-end mutes removed high-amplitude first arrivals, allowing trace balancing to enhance low-amplitude reflection information recorded later in the data. Coherent noise filtering removed most of the lateral system noise recorded in the regions below 40 ns in the data. Bandpass and frequency-wavenumber (f-k) filters reduced the lower frequency information and enhanced high-frequency reflections. Trace balancing via automatic gain controls (AGC) allowed some of the low-amplitude events to become more visible. The data were then elevation corrected to an arbitrary datum at the highest elevation along the line to remove the longer period elevation static shifts that inhibit correlation with the outcrop, and prevent the loss of any data. Therefore, the top of the data on the GPR sections roughly corresponds to the surface.

Interpretation of the data was aided by workstation-based interpretation software. Once in the workstation, reflective horizons and other boundaries were picked using the software. Various types of displays such as variable density, variable area-wiggle, and different color schemes were looked at as an aid to interpretation. Separate lines were also viewed simultaneously to allow correlation from one profile to another. Interpreted horizons were easy to change. Once completed, perspective views of the horizons of each data set were constructed to get a better picture of how the horizons on each line related to one another in three dimensions. Final sections of each line, including detailed views, were then printed and used as figures for this report.

RESULTS

General Results

Site maps of the study areas show the relationship between the GPR lines and the kimberlite outcrops (Figs. 2 and 3). The beginning and ending station numbers are indicated on the lines. Station locations are marked on the maps every 7.6 m (25 ft) by black dots. A cross-section across the Randolph 2 kimberlite based on outcrop and core data published by Brookins

(1970a) is shown in Figure 4. The interpreted GPR data from Randolph 1 are shown in Figures 5-10. Blow-ups of portions of lines R103, R105, and R106 are shown in Figures 11-13 respectively. Perspective views of the interpreted horizons of the Randolph 1 GPR data are shown in Figure 14. The interpreted GPR data from Randolph 2 are shown in Figures 15-19. A blow-up of a portion of line R204 is shown in Figure 20. Perspective views of the interpreted horizons of the Randolph 2 GPR data are shown in Figure 21. Uninterpreted copies of the GPR data shown in Figures 5-10 and 15-19 are placed in Appendix A. Station locations on the GPR data are indicated by vertical pulse lines on the sections every 1.5 m (5 ft) and double lines every 7.6 m (25 ft). The data are plotted down to approximately 70 ns below the surface. This corresponds to a depth of 4.3 m (14 ft) assuming an average one-way velocity of 0.12 m/ns (0.4 ft/ns), which is appropriate for limestone (Davis and Annan, 1989).

Interpreted reflective horizons on the GPR data are indicated by black lines (Figs. 5-21). These reflections occur within limestone members of the Permian Chase Group at both sites, and in some cases mark the contact between the limestone and overlying or underlying shale members. At the Randolph 1 site, the host limestone near the contact has been mapped as the Towanda Limestone Member of the Doyle Shale (see Figure 1 of Brookins, 1970a). Alternatively, this limestone may be the Cresswell Limestone Member of the Winfield Limestone (Brookins, 1970a and b). However, the recent Geologic Map of Riley County, Kansas (Smith and Archer, 1995) shows only the Barneston Limestone and Doyle Shale at the Randolph 1 site. In either case, the limestone member is still a limestone encased between shale members, so its stratigraphic level does not affect the interpretation. For the purposes of this report, the limestone is interpreted to be the Towanda Limestone Member of the Doyle Shale. At the Randolph 2 site, the host limestone near the contact is the Fort Riley Limestone Member of the Barneston Limestone.

The contacts between the kimberlite intrusions and host rock, as shown by Brookins (1970a), are also indicated by black lines on the GPR (Figs. 5-21). Only the surface location of the contact is based on the maps (Figs. 2 and 3). The dip of the contacts are speculative and based on general interpretation of the Riley County kimberlites (Brookins, 1970a and b), or in the case of Randolph 2, based on core samples near some lines (Brookins, 1970a) or the termination of reflections within the limestone host rock. At the Randolph 1 site, an alternative location for the kimberlite contact is also indicated based on termination of reflections on the GPR data.

Correlation of true reflections are complicated by instrument generated noise which creates events that are parallel to the top of the GPR data (elevation corrected surface) and extend downward throughout the data. Because of the AGC applied during processing, this noise is particularly apparent where the true reflective signal is weak or nonexistent. It is generally easy to ignore the noise when it cuts across the true reflections, but it may complicate interpretation when it is parallel or sub-parallel to the reflective fabric. A barbed wire fence at the Randolph 1 site, which

is perpendicular to the GPR lines along their southeast end (Fig. 2), does not appear to have any affect on the data. Likewise, trees near the lines at the Randolph 2 site do not appear to adversely affect the data either. Minor variations in soil thickness and velocity, as well as minor changes in topography that occur between elevation measurements, result in some of the short period static shifts or waviness exhibited by the GPR data. Some of this pattern, however, may also be due to intersecting diffractions (concave downward hyperbolas) caused by open or soil filled joints and other fractures near the surface, or irregularities in bedding surfaces within the limestone.

Randolph 1

At the Randolph 1 site, reflections on the GPR data are interpreted to occur within and at the base of the Towanda Limestone (Dt1-Dt4) (Figs. 5-13). Reflections are not observed within the kimberlite (Ka and possibly Kb). A detailed plot of line R103 between stations 100 and 140 (Fig 11), shows the typical character of these reflections within an area of nearly horizontal bedding. Four reflections have been interpreted on the six lines at this site, dividing the Towanda Limestone into four units (Dt1-Dt4), and what has been interpreted as the underlying Holmesville Shale Member (Dh). An exact correlation of the interpreted reflections between lines is not possible because of the lack of a cross line, but character ties and relative position of the reflections in time suggests that the correlations are reasonable. Although the Holmesville Shale is not shown on a map of the site (Fig. 2), it is interpreted to intersect the surface near station 140 on line R106 (Fig. 10). According to Jewett (1941), the thickness of the Towanda Limestone varies from less than a meter (a few feet) to more than 4.6 m (15 ft) throughout Riley County. Measurements of a core from the Amoco No. 1 Hargrave well in sec. 32, T. 7 S., R. 6 E. (Twiss, 1991), puts the Towanda Limestone at 5.5 m (18 ft) there. However, thicknesses of 2.3 m (7.6 ft) and 3.5 m (11.4 ft) reported from measured sections in the same Township as the Randolph 1 site (Jewett, 1941) suggests that the maximum preserved thickness of 2.4-3.0 m (8-10 ft), estimated from the GPR data for the Towanda Limestone at the Randolph 1 site, is reasonable, and that the base of the limestone occurs at the reflection between Dt4 and Dh (Figs. 5-13).

The reflectivity within the Towanda Limestone is probably due to minor lithologic changes between the beds or compaction differences which result in dielectric constant contrasts between the beds. The stronger reflections are due to larger dielectric constant contrasts or constructive interference of reflections from relatively thin beds. Numerous diffractions occur near the base of the Towanda Limestone in unit Dt4, and particularly at the contact between Dt4 and Dh. These diffractions may emanate from relatively abrupt irregularities along the bedding surfaces such as joints, small scale faults, or other fractures near the contact between the base of the Towanda Limestone and the Holmesville Shale. These diffractions, combined with the relatively high-

amplitude reflection between Dt4 and Dh, and the lack of reflectivity within Dh, support the interpretation that unit Dh is actually the Holmesville Shale. Several diffractions also occur with a possible velocity pull-down within unit Dt3 near station 135 (Fig. 11). These events may represent a 1.5 m (5 ft) wide near-surface collapse feature centered near station 135, with the apex of the diffractions marking the margins of the feature.

The Randolph 1 kimberlite intrusion is indicated on the GPR data by upward flexure of reflectors within the Towanda Limestone (Figs. 5-10). This folding is consistent with the forceful emplacement of the kimberlite, and is also indicated by dips in the limestone of 21°-45° near the kimberlite contact (Brookins, 1970a and b) (Fig. 2). According to Brookins (1970a), limestone dips become nearly horizontal a few feet away from the contact. According to the GPR data however, the dips do not flatten until 15.2-22.9 m (50-75 ft) away from the mapped contact of the kimberlite (Figs. 5-10). The hinge between the dipping and nearly horizontal beds may be fairly abrupt (Fig. 12) or relatively gentle (Fig. 13). Beds near the hinge may also show signs of smaller amplitude and wavelength folding (Fig. 12). However, this apparent folding may also be due static shifts caused by elevation differences which were unaccounted for in processing and display. Improper choice of a velocity for elevation static corrections may also have accentuate or suppressed the dip magnitude of the dipping reflections. This does not appear to be a problem at this site, because the nearly horizontal reflections at the northwest end of the line correlate with geologic dips (Brookins (1970a), even though there is a dipping ground surface.

Additional indirect evidence for the kimberlite intrusion comes from the up-dip termination of reflections from the limestone beds, particularly the shallower units (Figs. 5-10 and 13). The abruptness of the terminations is also indicated by diffractions trailing from the end of the reflections. An example of this is found on line R105 (Figs. 9 and 13) between stations 40 and 42.5 around 65 ns. Termination of these reflections may be due to the kimberlite contact, brecciation of the limestone beds to the point that coherent reflection events are no longer possible, or removal of the contrasts in dielectric constants by contact metamorphism. Another possible alternative is that the soil abruptly thickens to the point that the signal is completely attenuated. However, this is not observed at the site, and a gradual thickening of soil would cause the reflectivity to die out gradually, not abruptly. According to Brookins (1970b), pyrometamorphic contact effects are not noted, which leaves brecciation or the intrusive contact as possible alternatives. As mapped (Fig. 2), the margin of the kimberlite (Ka) is shown diagramatically as a steeply dipping contact 4.6-9.1 m (15-30 ft) southeast of the termination of the Towanda Limestone reflections (Figs. 5-10). An alternative intrusive contact based on the GPR data occurs at the termination of these reflections so that (Kb) represents kimberlite as well. This discrepancy could easily be explained by a slight mapping error. It is also possible that Kb represents a disturbed transition zone between 100% bedded limestone and 100% intrusion. Termination of

progressively deeper reflections farther away from the contact with Kb might suggest that the intrusion margin dips moderately to the northwest. However, this is opposite the steep east-southeast dips determined by magnetometer surveys for the Riley County kimberlite intrusions (Brookins, 1970a). A better explanation might be that the limestone beds become progressively broken up in the hinge area and dipping limb of the fold as they approach the kimberlite, particularly beds near the base of the limestone. This would cause increased scattering of the radar waves and less reflectivity from deeper beds as the signal-to-noise ratio increases. Greater attenuation of the signal beneath the dipping units may also be a result of the slightly thicker soil observed above the dipping units for all of the lines.

An excellent way to compare the interpretations on all the lines at once is through perspective views. Figure 14a shows the ground surface of all the lines, with the mapped intrusion margin for unit Ka and the possible GPR intrusion margin for unit Kb. Also shown is the interpreted horizon between units Dt2 and Dt3. Note that the limestone horizon is nearly horizontal on all the lines as it intersects the surface near the northwest end of the lines, and that it is bent upward as it approaches the kimberlite. Also note that the kimberlite contacts (both for Ka and Kb) and the upwarped limestone horizon are curved in plan view, indicating the elliptical shape of the intrusion and its effects on the margins of the host rock. The elliptical nature of the kimberlite margin and the effect of the forceful intrusion on the surrounding limestone beds are also indicated by the other perspective view in Figure 14b, which shows all the interpreted limestone horizons and the mapped kimberlite contact for unit Ka.

Randolph 2

Most of the GPR reflectivity at the Randolph 2 site (Fig. 3) occurs within the Fort Riley Limestone Member of the Barneston Limestone (Figs. 15-20). Reflections are also interpreted to occur from the top and base of the Fort Riley Limestone on some lines (Figs 15, 18-20). These interpreted reflections divide the GPR data into eight units: the Holmesville Shale Member of the Doyle Shale (H), six internal Fort Riley Limestone units (FtR1-FtR6), and the Oketo Shale Member of the Barneston Limestone (O) (Figs. 15-20). Like the correlations on the Randolph 1 data, exact correlations of interpreted reflections between lines are not possible because of the lack of data tying the reflections from one line to another. Reflection character and the time at which reflections occur on the sections suggest that the correlations are reasonable. The contact between the Randolph 2 kimberlite (K) and the surrounding host rock is also interpreted from projection of core data and the termination of limestone reflections (Figs. 15-20). As with the Randolph 1 site, internal reflections are not visible from the kimberlite. However, diffractions near the surface, possibly due to large xenoliths or other foreign blocks such as the host rock, are visible on lines

R201 and R203 (Figs. 15 and 17).

Although not exact, the reflection interpreted as the top of the Fort Riley Limestone on lines R204 and R205 (Figs. 18-20) correlates fairly well with the mapped contact between the Fort Riley Limestone and Holmesville Shale (Figs. 3). The change in character in the GPR signal from noise above the contact to reflections at and below is quite obvious on a blow up of a portion of line R204 (Fig. 20). The Holmesville Shale also appears to attenuate the GPR signal as indicated by the disappearance of underlying reflections as the thickness of the shale increases on lines R204 and R205 to the west (Figs. 18 and 19). Attenuation of the signal may also be due to thickening and/or increased conductivity of the soil. Reflectivity within the Fort Riley Limestone probably occurs for similar reasons as it does in the Towanda Limestone at the Randolph 1 site. In addition, lithologic descriptions of the Fort Riley Limestone from outcrop studies (Jewett, 1941) and the Amoco No. 1 Hargrave core (Twiss, 1991) suggest that the reflectivity may be accentuated by beds of dolomite, argillaceous limestone, calcareous shale, shale, and possibly evaporites. As close to the surface as the Fort Riley is when imaged on the GPR lines (no more than about 4.3 m; 14 ft), the evaporite beds may have been dissolved out, leaving a residual bed which may also be reflective. The reflection associated with the base of the Fort Riley Limestone on line R201 (Fig. 15) was picked mainly on the basis of approximate thickness of the limestone on the GPR data as determined from the drill holes at the site (Figs. 3 and 4). It is also the stratigraphically deepest reflection interpretable from the GPR data.

The drill hole data suggest that the Fort Riley Limestone beds are bent upward near the Randolph 2 kimberlite intrusion (Fig. 4) (Brookins, 1970a). However, unlike the Randolph 1 site where the GPR data clearly shows the folding, GPR data at the Randolph 2 site do not show a pronounced upwarping of reflectors. Lines R203-R205 (Figs. 17-20) do show reflections dipping away from the kimberlite intrusion, however, lines R201 and R202 (Figs. 15 and 16) show dips toward the kimberlite. In all cases the dips are much gentler than imaged on the Randolph 1 data. One possible reason for the unexpected dips on lines R201 and R202 may be due to improper elevation corrections. It is possible that the velocity used for the elevation statics correction was too high for that portion of the data. A lower velocity would increase the slope of the surface in time, and flatten the westward dips or cause them to dip eastward. If this lower velocity is applied to lines R204 and R205 though, the dips on those lines would also flatten, causing a reduction in dip away from the kimberlite. Alternatively, the westward dips on lines R201 and R202 are real, and the drill hole on the eastern margin of the intrusion is too close to the kimberlite to correlate with the observed reflectivity (Figs. 3, 4, 15, 16), or that the drill hole does not contain enough information for a dip determination. Close observation of line R201 (Fig. 15) does reveal that the westward dip of reflections increases from the northeast end of the line towards the intrusion. This is particularly evident from reflections bounding unit FtR5. It is possible that an abrupt upward

bend at the base of FtR3 occurs near the kimberlite contact (Fig 15). It is also possible that the upward bending is not completely imaged by the GPR data east of the intrusion since most of the reflections on lines R201 and R202 terminate several feet before they intersect the proposed kimberlite contact. Like the reflections at the Randolph 1 site, the terminations may be due to signal attenuation, brecciation of the beds, or the intrusive contact of the kimberlite.

Perhaps the best indicator of the margin of the kimberlite on most of the lines at this site is the truncation of at least the shallower reflections. This relationship is probably best demonstrated by lines R203-R205 (Figs. 17-20). Diffractions are also observed at and near some of these truncations (e.g. diffractions above unit FtR4 near station 25 on line R203; Figure 17). Unlike the Randolph 1 site, where all the reflections terminated before the mapped contact of the kimberlite, reflections on lines R203-R205 come very close to, or extend below the mapped surface contact of the kimberlite intrusion (Figs. 17-20). This is best shown on a blow-up of a portion of line R204 (Fig. 20). On this line, the approximate margin of the kimberlite is defined by projection of the drill hole data (Figs. 3 and 4). Reflections from both the top and base of unit FtR1 appear to extend beneath the kimberlite outcrop and terminate at a position close to the kimberlite margin in the subsurface. Therefore, it is likely that the termination of these reflections marks the subsurface contact with the kimberlite. In addition, a reflection between stations 30 and 45 on line R204 (Fig. 20) also appears to correlate with the kimberlite contact. The reason that a reflection associated with the contact may be seen here and not elsewhere may be that the contact is too steep elsewhere to be imaged by the GPR unit with the acquisition parameters used. It is also possible that this shallower, flatter portion of the kimberlite contains material that has a dielectric constant different enough from the limestone to cause a reflection.

As with the Randolph 1 site, the best way to view the interpreted limestone horizons and kimberlite contact on all the lines simultaneously at this site is with perspective views (Fig. 21). Figure 21a shows the ground surface of the lines, the margin of the kimberlite intrusion, and interpreted horizons between units H and FtR4. Figure 21b shows the ground surface, kimberlite intrusion, and interpreted horizons between units FtR4 and O. The mushroom-like shape of the kimberlite intrusion is evident on both perspective views. The general eastward slope of the ground surface at this site, except for the knoll associated with the intrusion, is also indicated. The dip of interpreted horizons away from the kimberlite on the west and south side, as well as the termination of horizons against the margin of the kimberlite, are easily seen on Figure 21a. The westward dip of reflectors to the east of the kimberlite is seen on Figure 21a and 21b. Note that most of these reflections terminate before intersecting the projected contact of the kimberlite, leaving room for the possible up-bending of beds near the intrusion on the east side, but not directly supporting it.

CONCLUSIONS

High-resolution ground-penetrating radar (GPR) was successful at imaging the near-surface margins of the Randolph 1 and Randolph 2 kimberlites to lateral distances of within 7.6 m (25 ft) in most cases, and probably less than 1 m (3 ft) in others.

The margins of a kimberlite intrusion can be identified on GPR by upward bending of reflective beds in the host rock as the intrusion is approached, and termination of reflections associated with these beds somewhere near, but not necessarily at, the intrusive contact. In many cases, the termination occurs below the kimberlite outcrop, indicating a dip of the kimberlite contact towards the center of the intrusion. Diffractions will often occur at the termination of reflections when the termination of beds associated with the reflections is abrupt, such as at the kimberlite contact.

Reflections do not occur from within the kimberlite, although diffractions are possible, probably from large xenoliths or other foreign blocks incorporated within the intrusion. In most cases, reflections are not observed from the kimberlite contact, probably because the contact is usually too steep or diffuse. However, a reflection may occur where the contact is gently dipping.

Reflectivity at both these sites is most pronounced from the top, base, and within the limestone host rock. The shale units are non-reflective, and attenuate the GPR signal as their thickness increases. An increase in the thickness of conductive soils may also increase signal attenuation. Diffractions are sometimes visible within and at the boundaries of limestone beds. These are probably due to the presence of joints, small scale faults, collapse features, or other fractures, and are more pronounced where the limestone beds are folded or adjacent to shales.

High-resolution GPR is a useful tool for delineating the margins of kimberlite intrusions (or other intrusions) down to depths of 4.3 m (14 ft) or more where the host rock contains limestone or other bedded units that are reflective. Lower frequency antennas may help extend the image depth, but would do so at the cost of resolution. High-resolution GPR may not be useful in areas of relatively thick, conductive soil, or where shale is at the surface.

ACKNOWLEDGMENTS

We would like to thank Dr. Neil Anderson from the University of Missouri-Rolla, for the use of UMR's GPR equipment, and Tim Carr for making Kansas Geological Survey funds available for the survey. We would also like to thank the Landmark Graphics Co. for the use of their SeisWorks/2D software through an educational grant to the Kansas Geological Survey.

REFERENCES

Berendsen, P., Cullers, R. L., Mansker, W. L., and Cole, G. P., 1985, Late Cretaceous kimberlite and lamproite occurrences in eastern Kansas, U.S.A.[Abstract]: Geological Society of America, Abstract with Programs, v.17, no. 3, p.151.

Berendsen, P., and Blair, K. P., 1992, Midcontinent Rift System, Precambrian structure map: Kansas Geological Survey, Open-File report 92-41A.

Brookins, D. G., 1970a, Factors governing the emplacement of Riley County, Kansas, kimberlites: Kansas Geological Survey Bulletin, no. 199, pt. 4, 17 p.

Brookins, D. G., 1970b, The kimberlites of Riley County, Kansas: Kansas Geological Survey Bulletin, no. 200, 32 p.

Brookins, D. G., and Naeser, C. W., 1971, Age of emplacement of Riley County, Kansas, kimberlites and a possible minimum age for the Dakota Sandstone: Geological Society of America Bulletin, v. 82, p. 1723-1726.

Byrne, F. E., Parish, K. L., and Crumpton, C. F., 1956, Igneous intrusions in Riley County, Kansas: American Association of Petroleum Geologists Bulletin, v.40, p. 377-387.

Davis, J. L. and Annan, A. P., 1989, Ground-penetrating radar for high-resolution mapping of soil and rock stratigraphy: Geophysical Prospecting, v. 37, p. 531-551.

Jewett, J. M., 1941, The geology of Riley and Geary Counties, Kansas: Kansas Geological Survey, Bulletin, no. 39, 164 p.

Jewett, J. M., 1951, Geologic structures in Kansas: Kansas Geological Survey Bulletin, no. 90, pt. 6. p. 105-172.

Mansker, W. L., Richards, B. D., and Cole, G. P., 1987, A note on newly discovered kimberlites in Riley County, Kansas: Geologic Society of America Special Paper, no. 215, p 197-204.

Smith, B. D. and Archer, A. W., 1995, Geologic map of Riley county, Kansas: Kansas Geological Survey, Map M-36, scale 1:50,000.

Telford, W. M., Geldart, L. P., Sheriff, R. E., and Keys, D. A., 1976, Applied Geophysics: Cambridge University Press, New York, New York, 860 p.

Twiss, P. C., 1991, Chase Group from the near-surface Amoco No. 1 Hargrave core, Riley County, Kansas; *in*, Midcontinent Core Workshop, Integrated Studies of Petroleum Reservoirs in the Midcontinent: Kansas Geological Survey, prepared for the American Association of Petroleum Geologists Midcontinent Section Meeting, Wichita, Kansas, p. 1 23-141.

FIGURES

Figure 1: Map of Riley County, Kansas, showing locations of the Randolph 1 (R1) and Randolph 2 (R2) kimberlites. Also shown are the 1, Bala; 2, Leonardville; 3, Stockdale; and 4, Winkler kimberlites, as well as the axis of the Abilene Anticline (modified from Figure 1 of Brookins, 1970b).

Figure 2: Geologic map of the Randolph 1 kimberlite, SW NW sec. 35, T 6 S, R 6 E, Riley County, Kansas, including locations of GPR lines with stations 0 and 150 marked on lines R101 and R106 (modified from Figure 1 of Brookins, 1970a).

Figure 3: Geologic map of the Randolph 2 kimberlite, SW SE sec. 35, T 6 S, R 6 E, Riley County, Kansas, including locations of GPR lines with the beginning and ending stations indicated (modified from Figure 2 of Brookins, 1970a). Note that station 0 is the same for each line and is located at approximately the same location as power auger drill site 2.

Figure 4: Generalized cross section of the Randolph 2 kimberlite showing projected locations and depths of power auger drill sites (from Figure 3 of Brookins, 1970a).

Figures 5-10: Variable density time sections of the GPR data for lines R101 through R106 at the Randolph 1 kimberlite site. Black reflections = highest amplitude peaks; white reflections = highest amplitude troughs. Gray = intermediate amplitudes grading from white to black. Vertical scale in nanoseconds (ns) horizontal scale in feet. Trace numbers are also listed across the top. Station locations every 1.5 m (5 ft) are indicated on the data by vertical pulses but are difficult to see on these sections. Data have been elevation corrected to a flat datum at the highest elevation of the survey lines. Interpreted horizons are marked with black lines separating the following units: Ka - mapped kimberlite intrusion, Kb - possible kimberlite or fractured limestone as interpreted from the GPR data, Dt1 through Dt4 - units within the Towanda Limestone Member of the Doyle Shale, Dh - Holmesville Shale Member of the Doyle Shale. Line locations are shown on Figure 2. Uninterpreted versions of these figures are shown in Appendix A.

Figure 11: Variable amplitude wiggle detailed section of line R103 of the Randolph 1 site between stations 104 and 140. Unit abbreviations are the same as Figures 5-10.

Figure 12: Variable amplitude wiggle detailed section of line R106 of the Randolph 1 site between stations 35 and 75. Unit abbreviations are the same as Figures 5-10.

Figure 13: Variable amplitude wiggle detailed section of line R105 of the Randolph 1 site between stations 35 and 75. Unit abbreviations are the same as Figures 5-10.

Figure 14: Perspective views of the horizons interpreted at the Randolph 1 site looking north..
a) Horizons shown are: ground surface; margin of the mapped kimberlite (Ka) and its possible contact at depth; margin of the possible kimberlite or highly fractured limestone (Kb) and its contact at depth; reflector between units Dt2 and Dt3 in the Towanda Limestone.
b) Horizons shown are: margin of the mapped kimberlite (Ka) and its possible contact at depth; all the reflectors separating units within the Towanda Limestone (Dt1-Dt4), and at the top of the Holmesville Shale (Dh).

Figures 15-19: Variable density time sections of the GPR data from lines R201 through R205 at the Randolph 2 kimberlite site. Black reflections = highest amplitude peaks; white reflections = highest amplitude troughs. Gray = intermediate amplitudes grading from white to black. Vertical scale in nanoseconds (ns) horizontal scale in feet. Trace numbers are also listed across the top. Station locations every 1.5 m (5 ft) are indicated on the data by vertical white lines, double lines every 7.6 m (25 ft). Data have been elevation corrected to a flat datum at the highest elevation of the survey lines. Interpreted horizons are marked with black lines separating the following units: K - mapped kimberlite intrusion, H - Holmesville Shale Member of the Doyle Shale, FtR1 through FtR6 - units within the Fort Riley Limestone Member of the Barneston Limestone, O - Oketo Shale Member of the Barneston Limestone. Line locations are shown on Figure 3. Uninterpreted versions of these figures are shown in Appendix A.

Figure 20: Variable amplitude wiggle detailed section of line R204 of the Randolph 2 site between stations 25 and 65. Unit abbreviations are the same as Figures 15-19.

Figure 21: Perspective views of the horizons interpreted at the Randolph 2 site looking northwest..
a) Horizons shown are: ground surface; margin of the mapped kimberlite (K); reflector at the base of the Holmesville Shale (H); and reflectors between units FtR1 and FtR4 in the Fort Riley Limestone.
b) Horizons shown are: ground surface; margin of the mapped kimberlite (K); reflectors between units FtR4 and FtR6 in the Fort Riley Limestone; and the reflector at the top of the Oketo Shale (O)

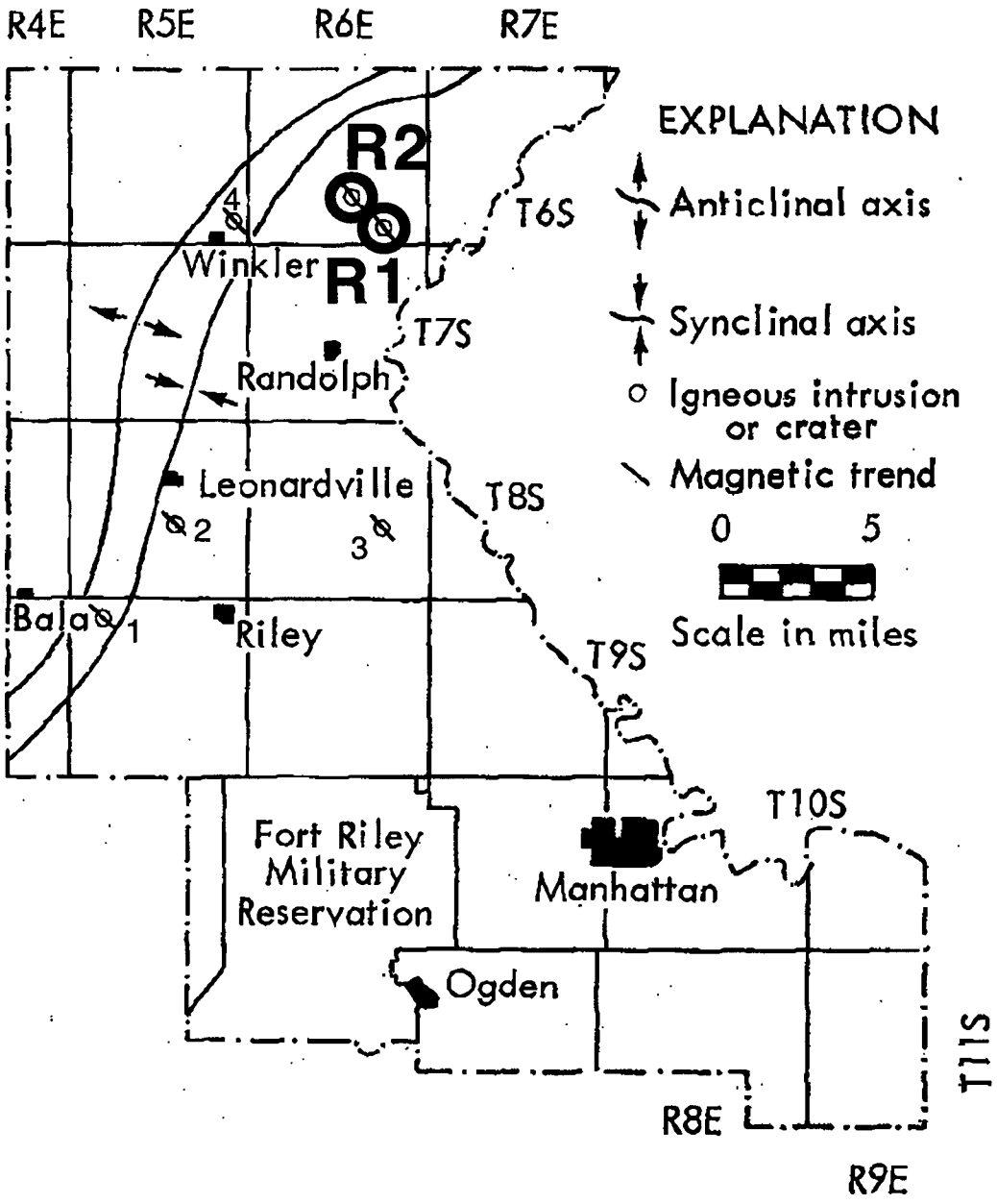
R4E
R5E
R6E
R7E
EXPLANATION
Anticlinal axis
Synclinal axis
Igneous intrusion or crater
Magnetic trend
0
5
Scale in miles
R2
R1
4
Winkler
T6S
T7S
Randolph
Leonardville
T8S
2
3
Bala
1
Riley
T9S
T10S
Fort Riley Military Reservation
Manhattan
Ogden
T11S
R8E
R9E

Figure 1

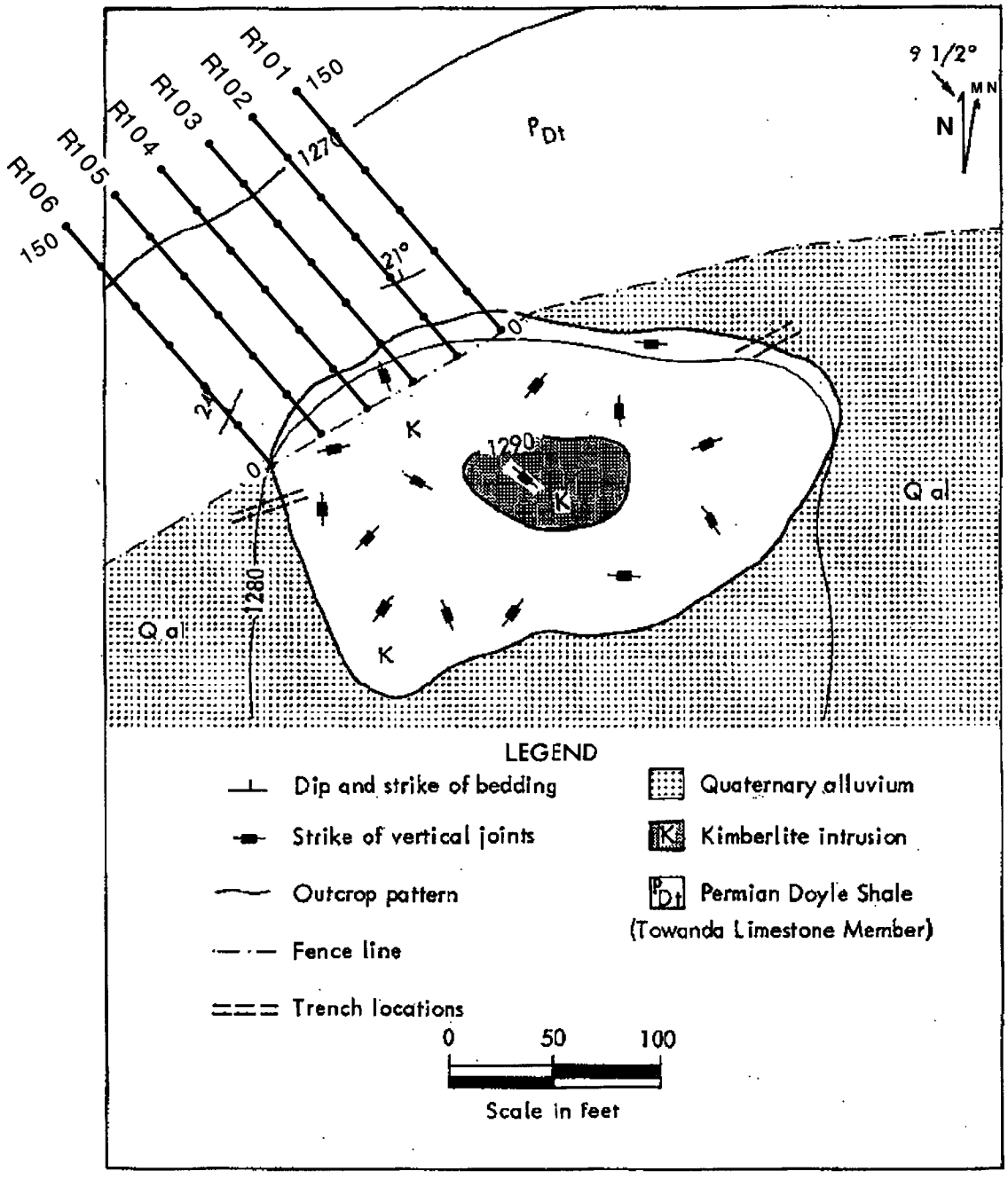
R101
R102
R103
R104
R105
R106
150
127
21°
0
24
0
1290
1280
K
K
K
P_{Dt}
Q al
Q al
9 1/2°
MN
N
LEGEND
Dip and strike of bedding
Strike of vertical joints
Outcrop pattern
Fence line
Trench locations
Quaternary alluvium
Kimberlite intrusion
Permian Doyle Shale
(Towanda Limestone Member)
0
50
100
Scale in feet

Figure 2

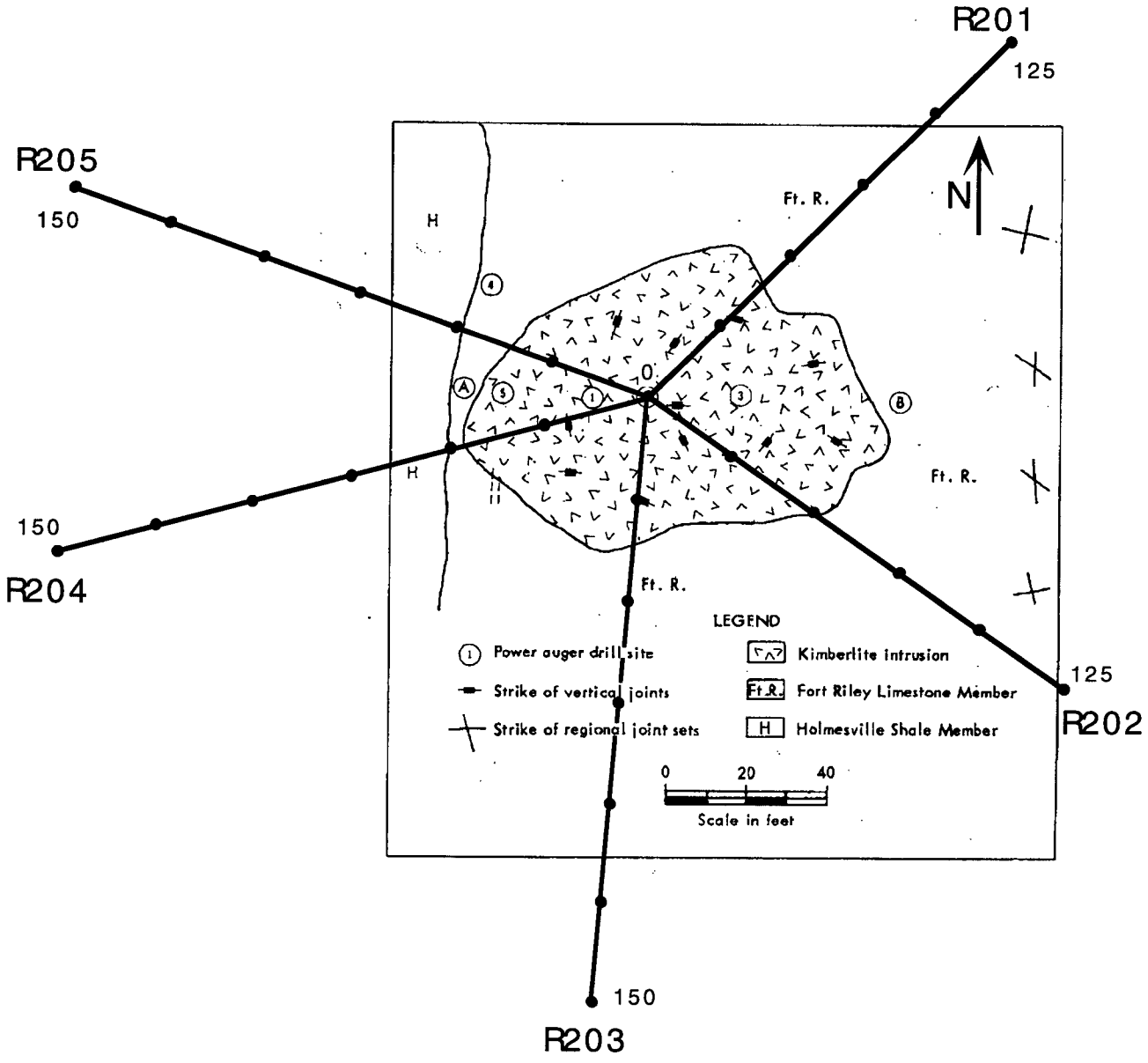
R201
125
R205
150
N
H
Ft. R.
4
A
5
1
2
3
B
H
150
R204
Ft. R.
Ft. R.
LEGEND
1 Power auger drill site
Strike of vertical joints
Strike of regional joint sets
Kimberlite intrusion
Ft.R. Fort Riley Limestone Member
H Holmesville Shale Member
0 20 40
Scale in feet
125
R202
150
R203

Figure 3

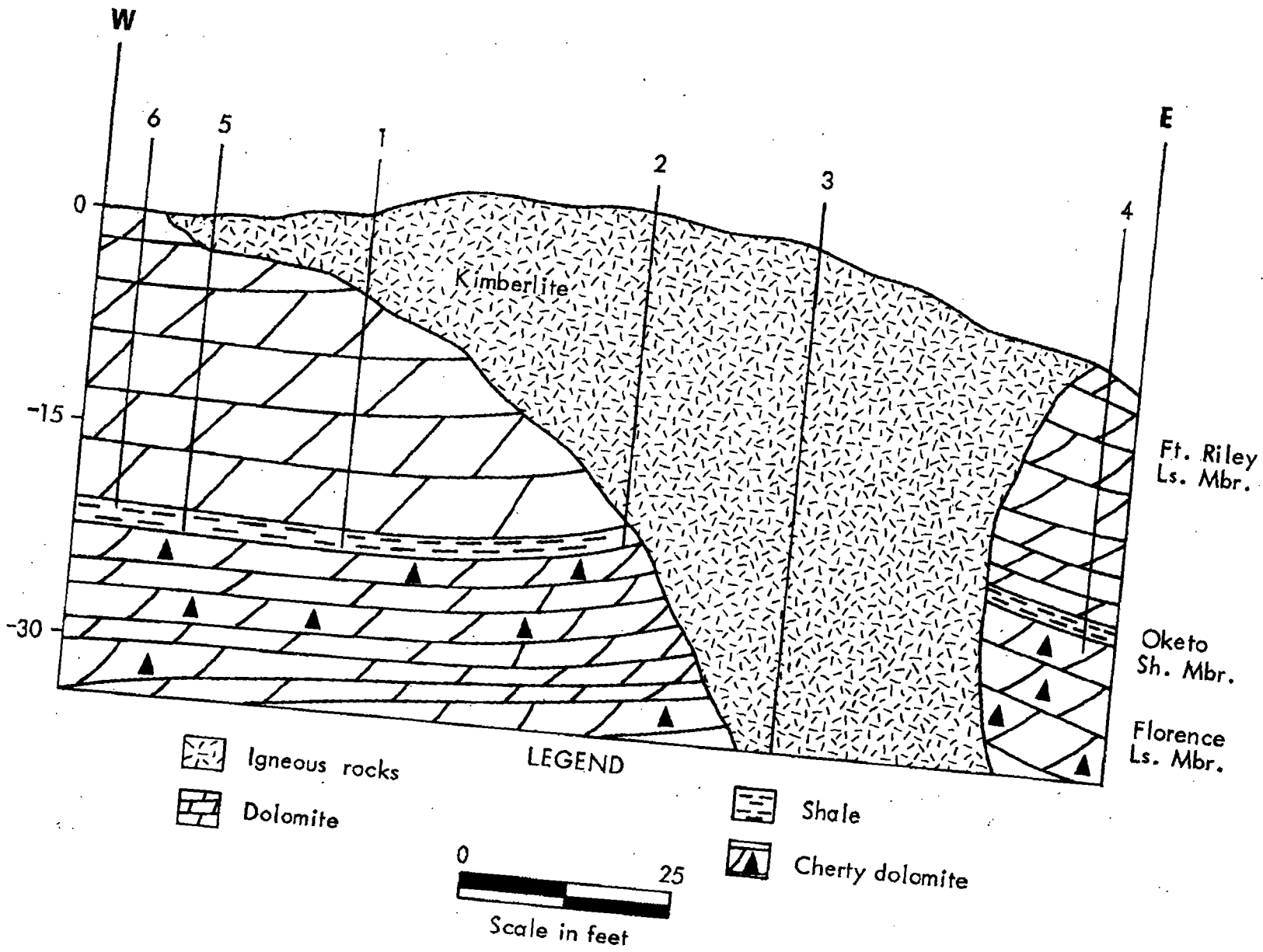
W
E
6
5
1
2
3
4
0
-15
-30
Kimberlite
Ft. Riley
Ls. Mbr.
Oketo
Sh. Mbr.
Florence
Ls. Mbr.
LEGEND
Igneous rocks
Dolomite
Shale
Cherty dolomite
0
25
Scale in feet

Figure 4

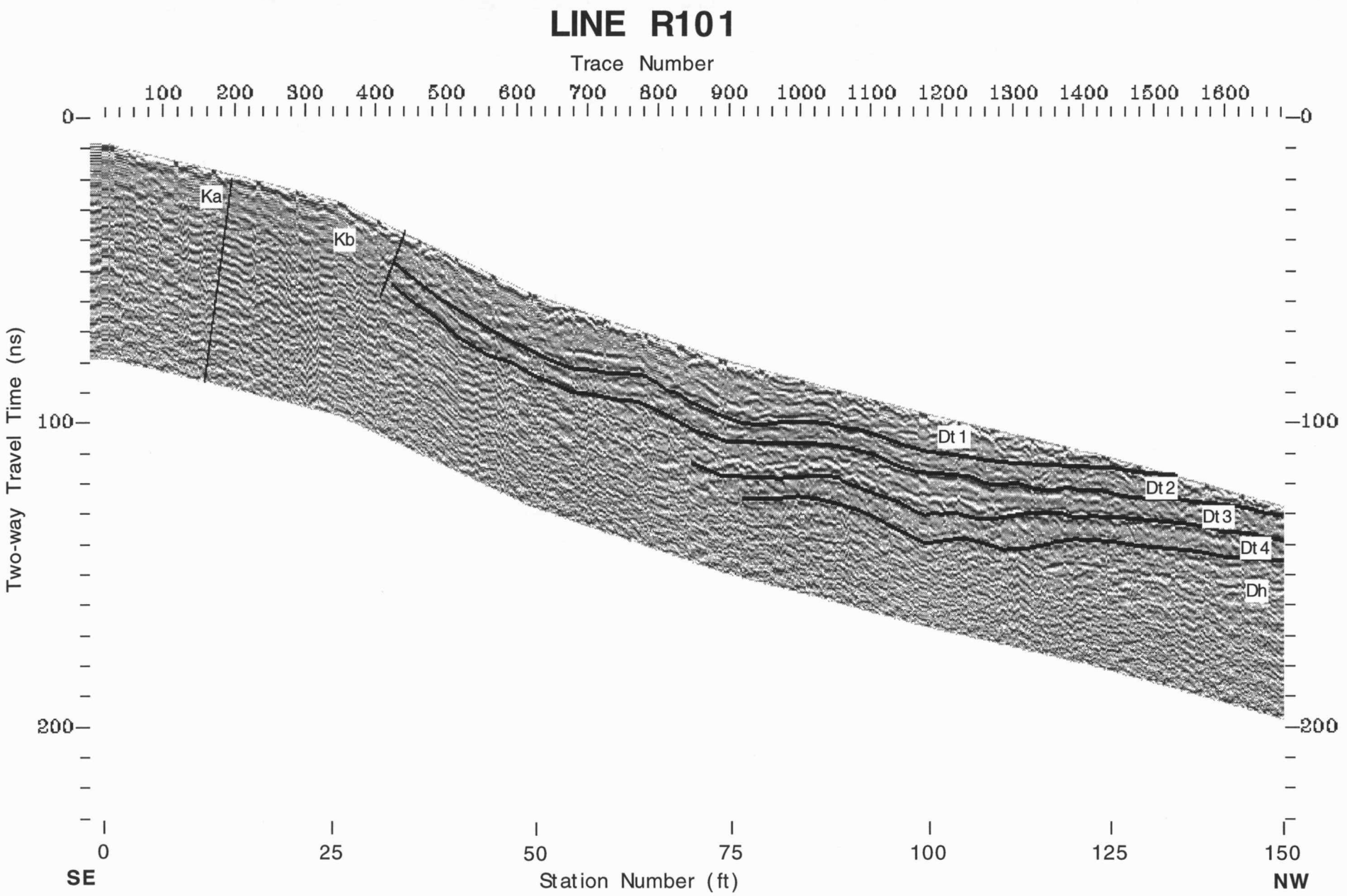
LINE R101
Trace Number
100 200 300 400 500 600 700 800 900 1000 1100 1200 1300 1400 1500 1600
0
100
200
Two-way Travel Time (ns)
Ka
Kb
Dt 1
Dt 2
Dt 3
Dt 4
Dh
0 25 50 75 100 125 150
SE
Station Number (ft)
NW

Figure 5

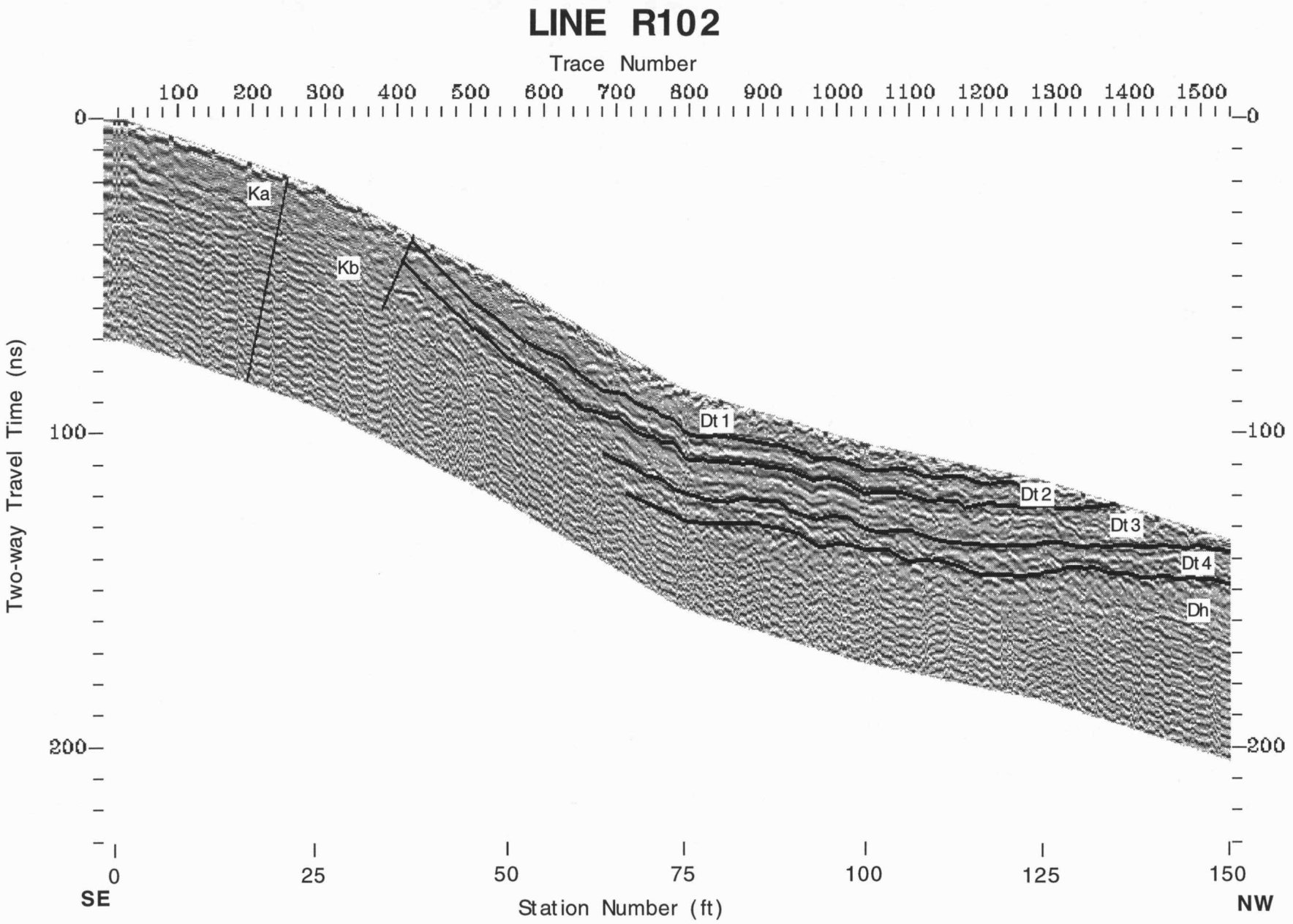
LINE R102
Trace Number
100 200 300 400 500 600 700 800 900 1000 1100 1200 1300 1400 1500
0
100
200
Two-way Travel Time (ns)
Ka
Kb
Dt 1
Dt 2
Dt 3
Dt 4
Dh
0 25 50 75 100 125 150
SE
Station Number (ft)
NW

Figure 6

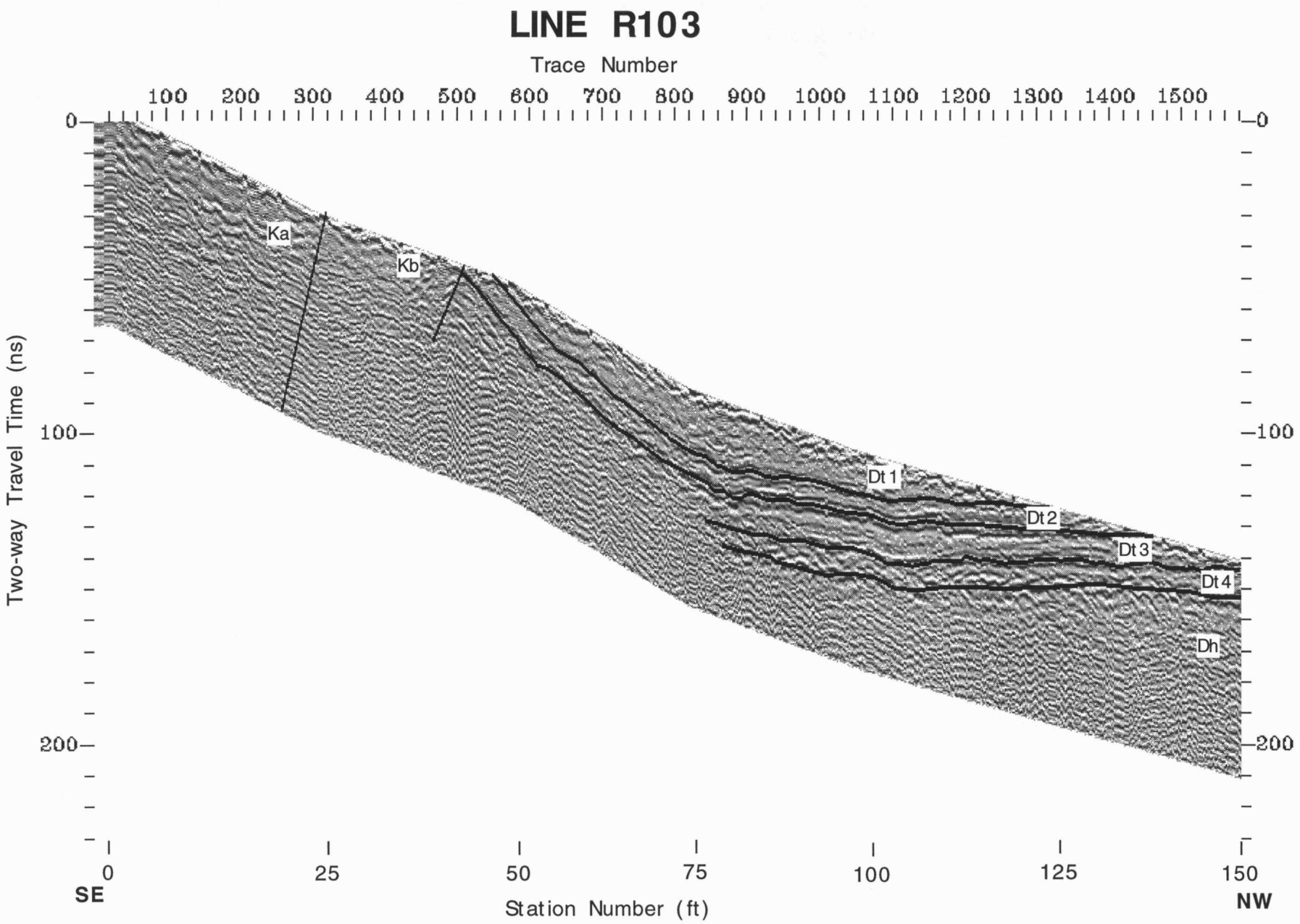
LINE R103
Trace Number
100 200 300 400 500 600 700 800 900 1000 1100 1200 1300 1400 1500
0
100
200
Two-way Travel Time (ns)
Ka
Kb
Dt 1
Dt 2
Dt 3
Dt 4
Dh
0 25 50 75 100 125 150
SE
NW
Station Number (ft)

Figure 7

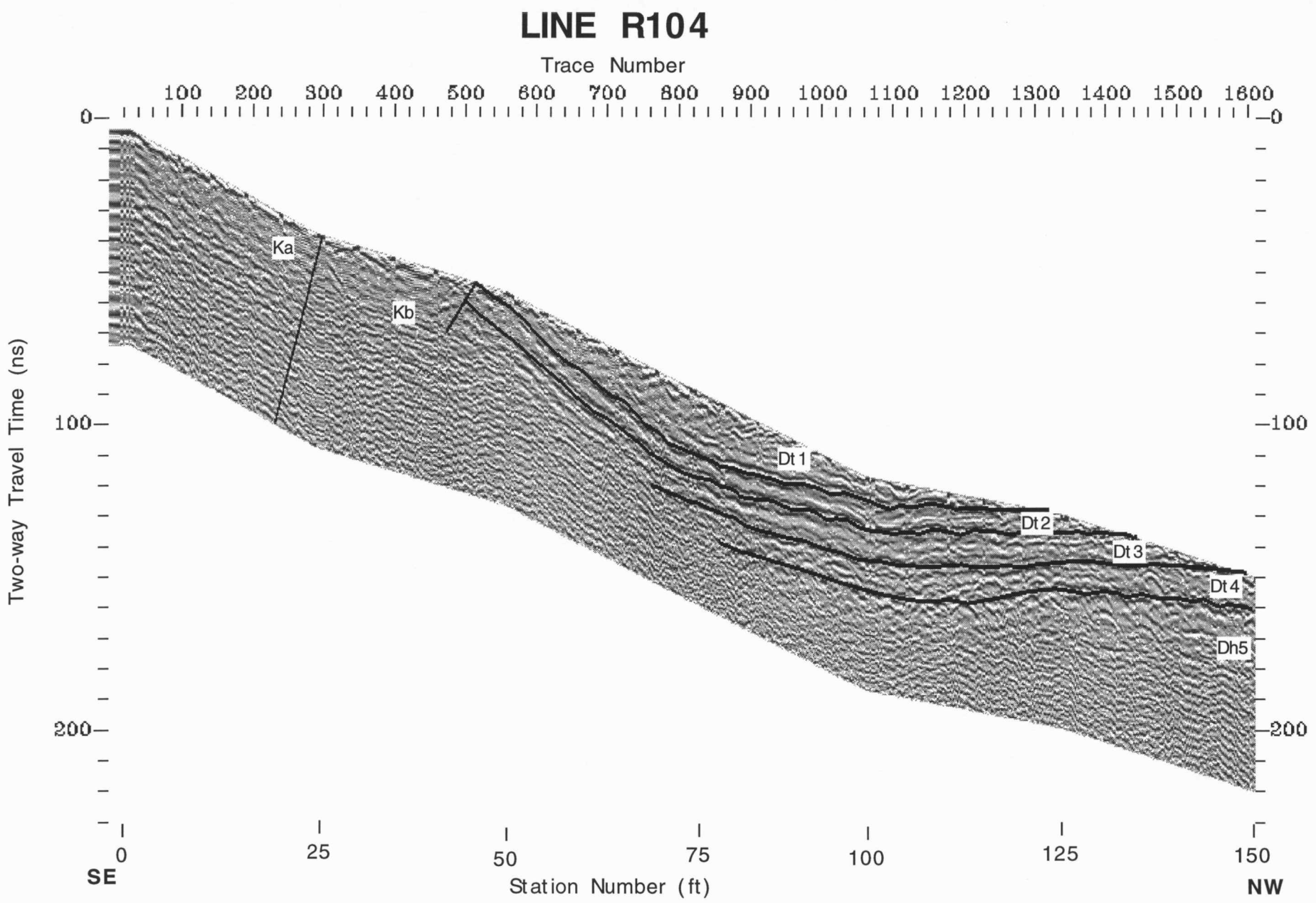
LINE R104
Trace Number
100 200 300 400 500 600 700 800 900 1000 1100 1200 1300 1400 1500 1600
0
100
200
Two-way Travel Time (ns)
Ka
Kb
Dt 1
Dt 2
Dt 3
Dt 4
Dh5
0 25 50 75 100 125 150
SE
Station Number (ft)
NW

Figure 8

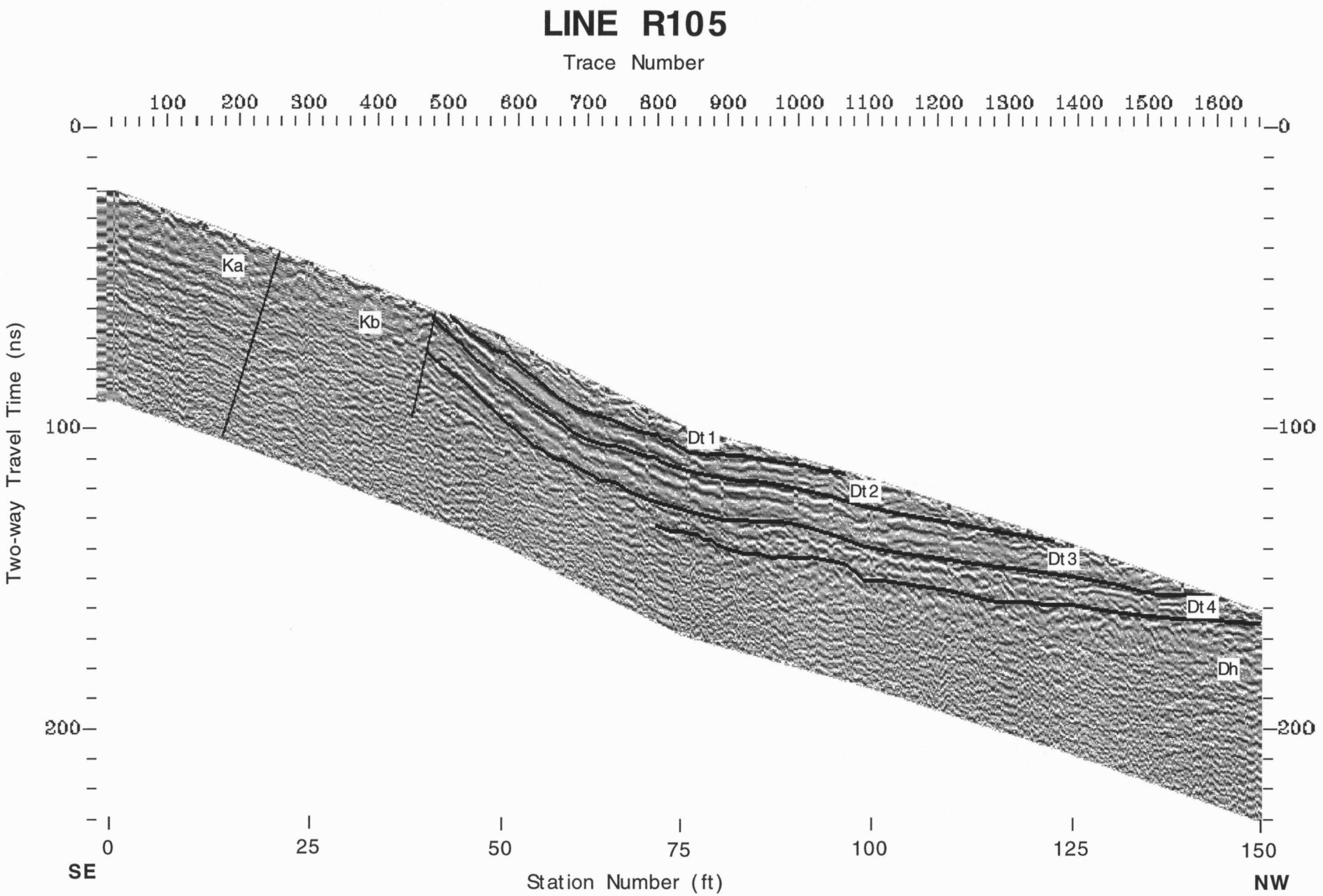
LINE R105
Trace Number
100 200 300 400 500 600 700 800 900 1000 1100 1200 1300 1400 1500 1600
0
100
200
Two-way Travel Time (ns)
Ka
Kb
Dt 1
Dt 2
Dt 3
Dt 4
Dh
0 25 50 75 100 125 150
SE
NW
Station Number (ft)

Figure 9

LINE R106

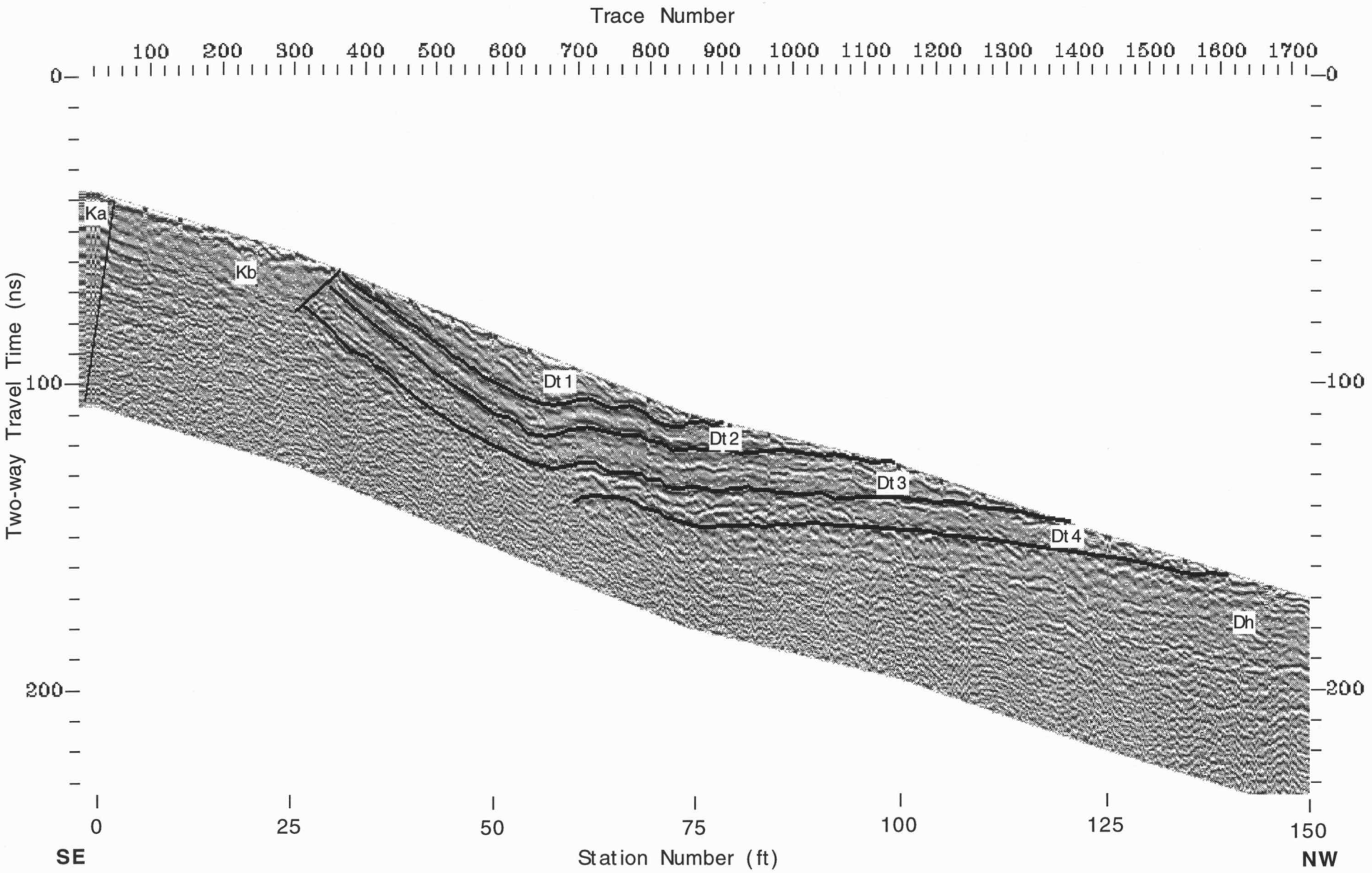

Figure 10

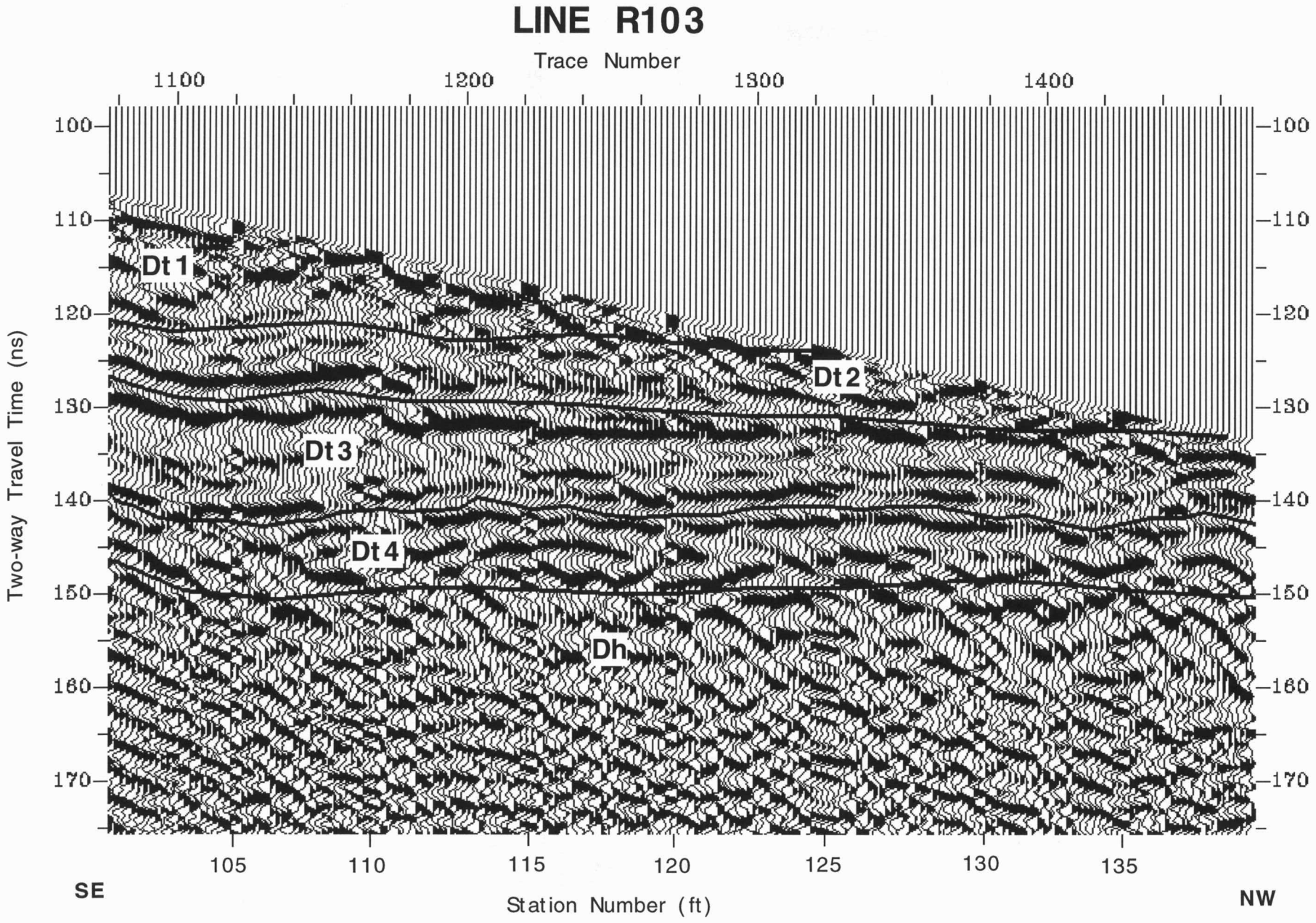
LINE R103
Trace Number
1100
1200
1300
1400
100
110
120
130
140
150
160
170
Dt 1
Dt 2
Dt 3
Dt 4
Dh
Two-way Travel Time (ns)
105
110
115
120
125
130
135
SE
NW
Station Number (ft)

Figure 11

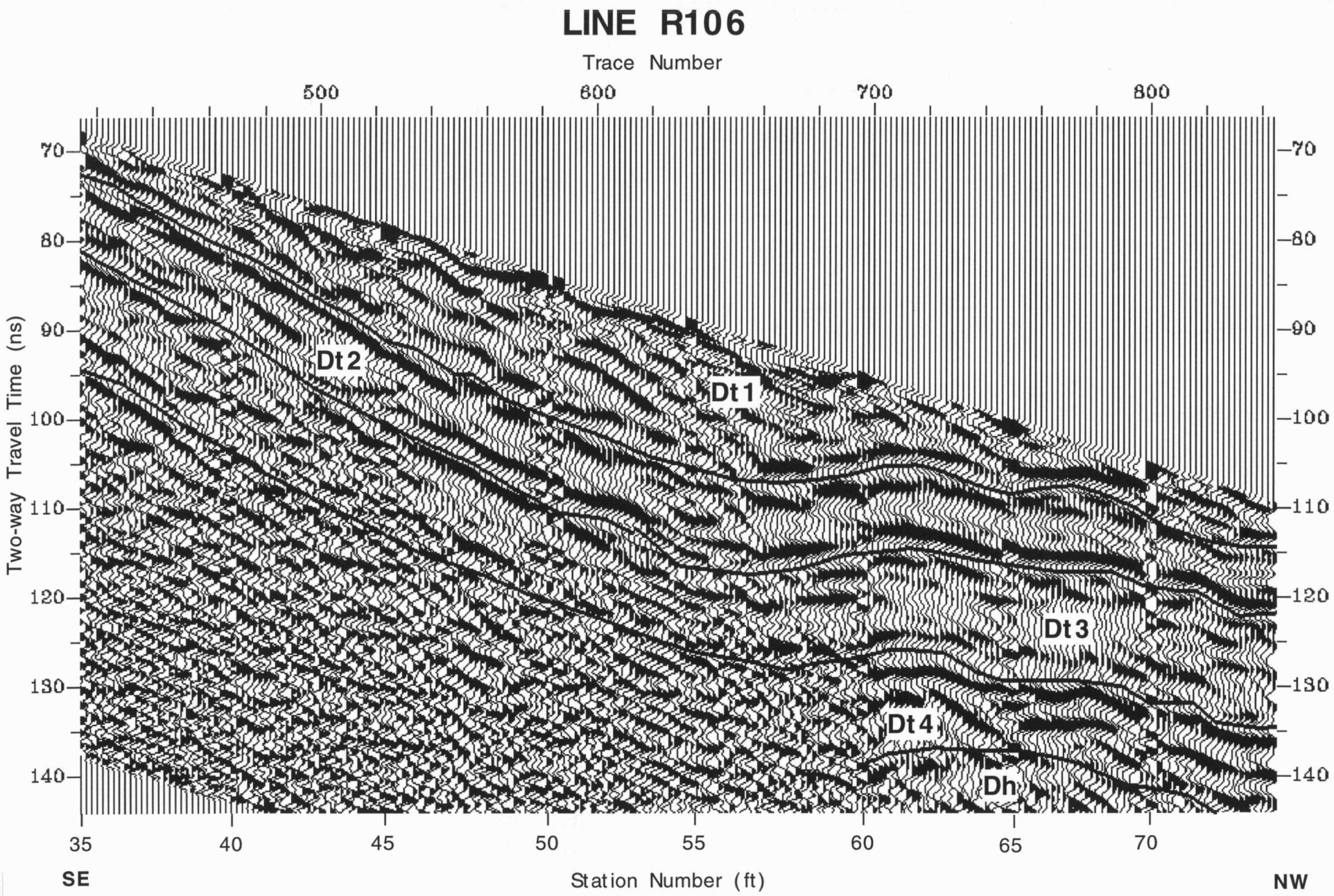
LINE R106
Trace Number
500
600
700
800
70
80
90
100
110
120
130
140
Two-way Travel Time (ns)
Dt 2
Dt 1
Dt 3
Dt 4
Dh
35
40
45
50
55
60
65
70
SE
Station Number (ft)
NW

Figure 12

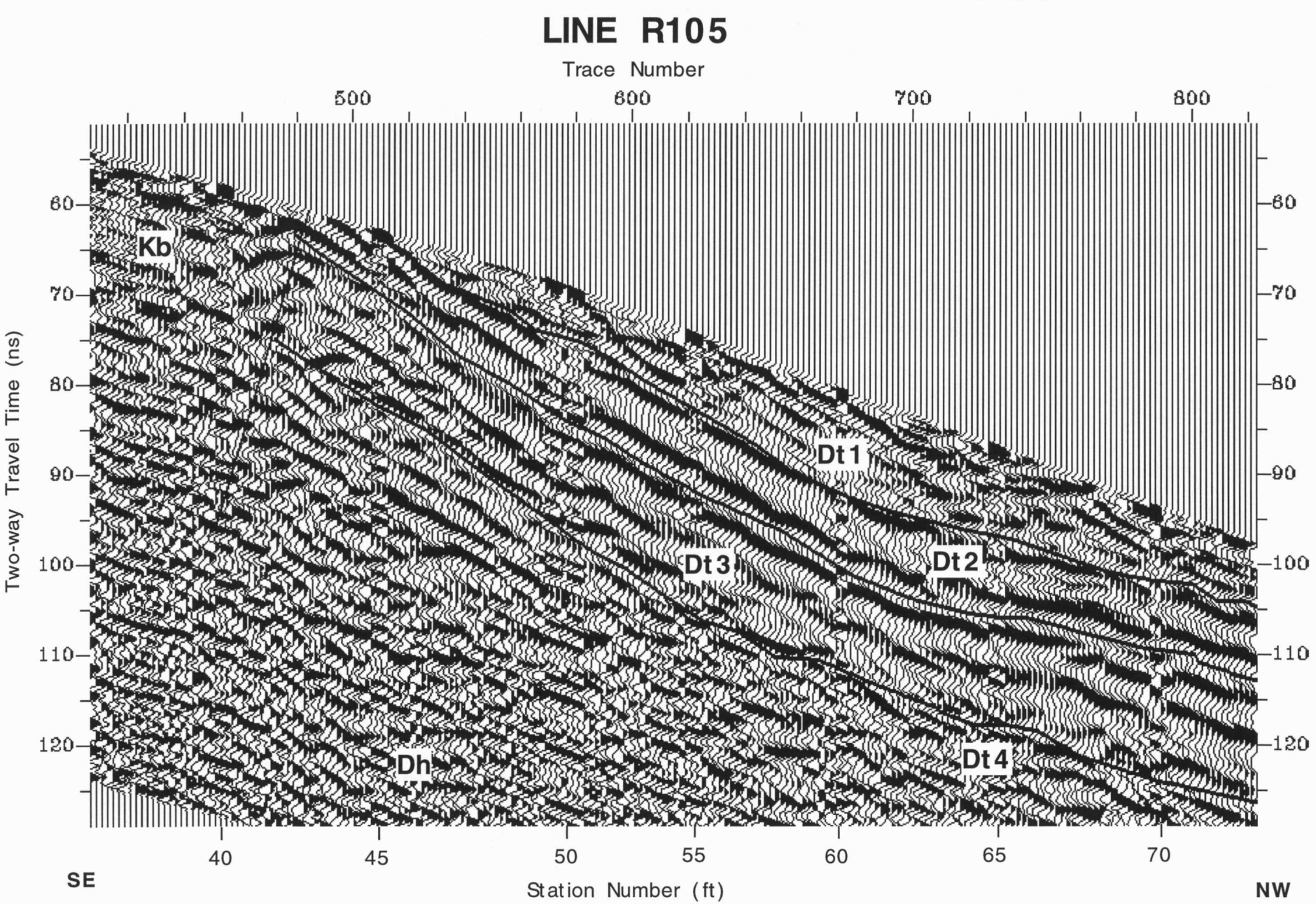
LINE R105
Trace Number
500
600
700
800
60
70
80
90
100
110
120
Two-way Travel Time (ns)
Kb
Dt 1
Dt 3
Dt 2
Dh
Dt 4
40
45
50
55
60
65
70
SE
Station Number (ft)
NW

Figure 13

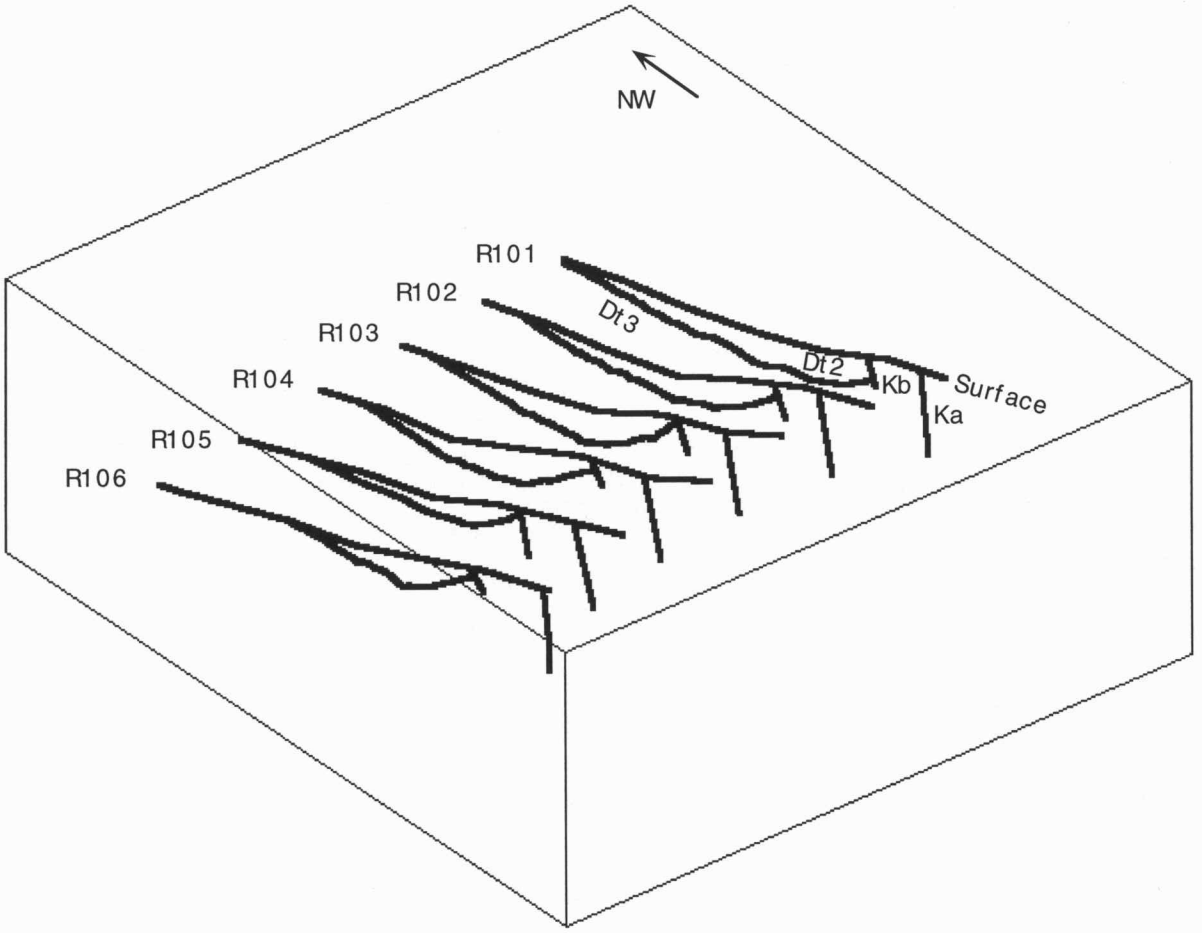

Figure 14a

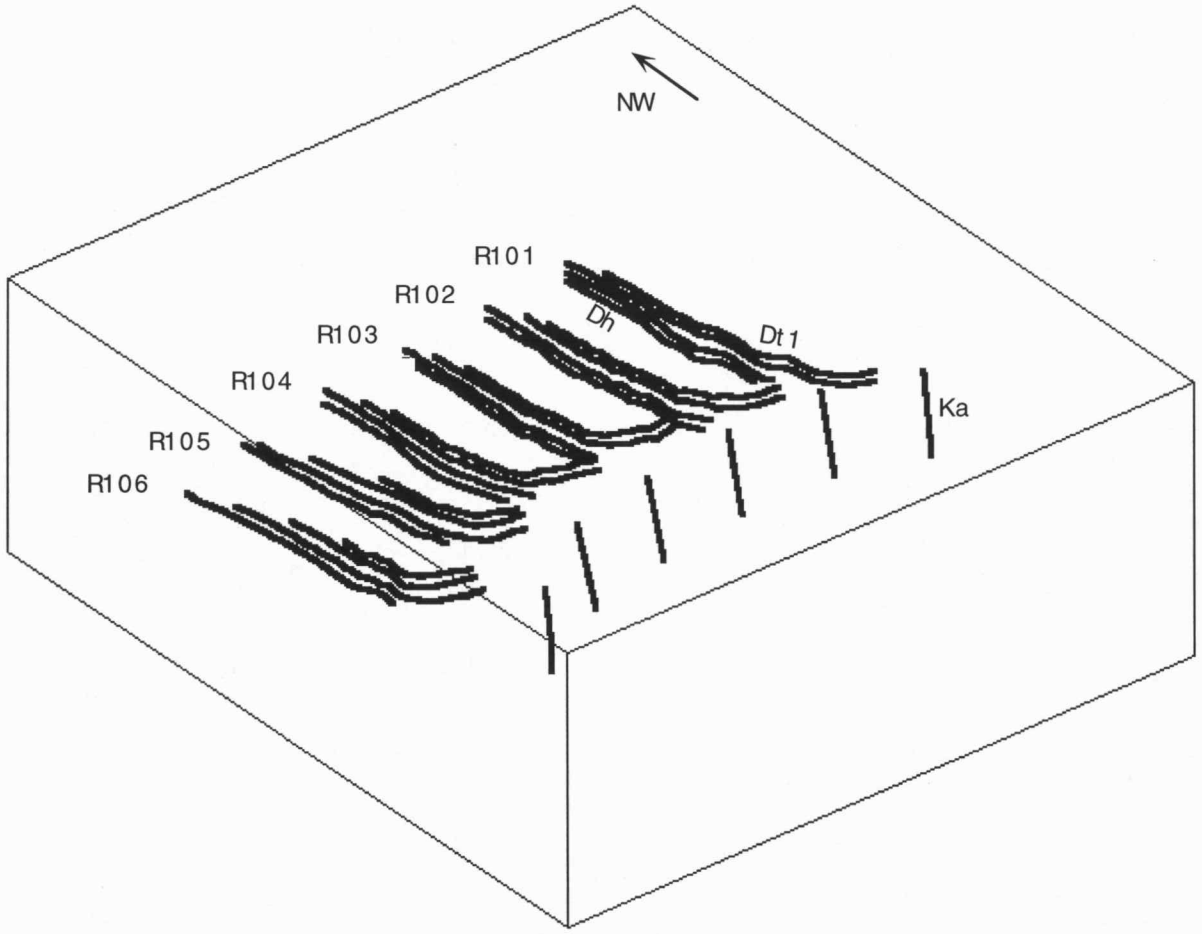

Figure 14b

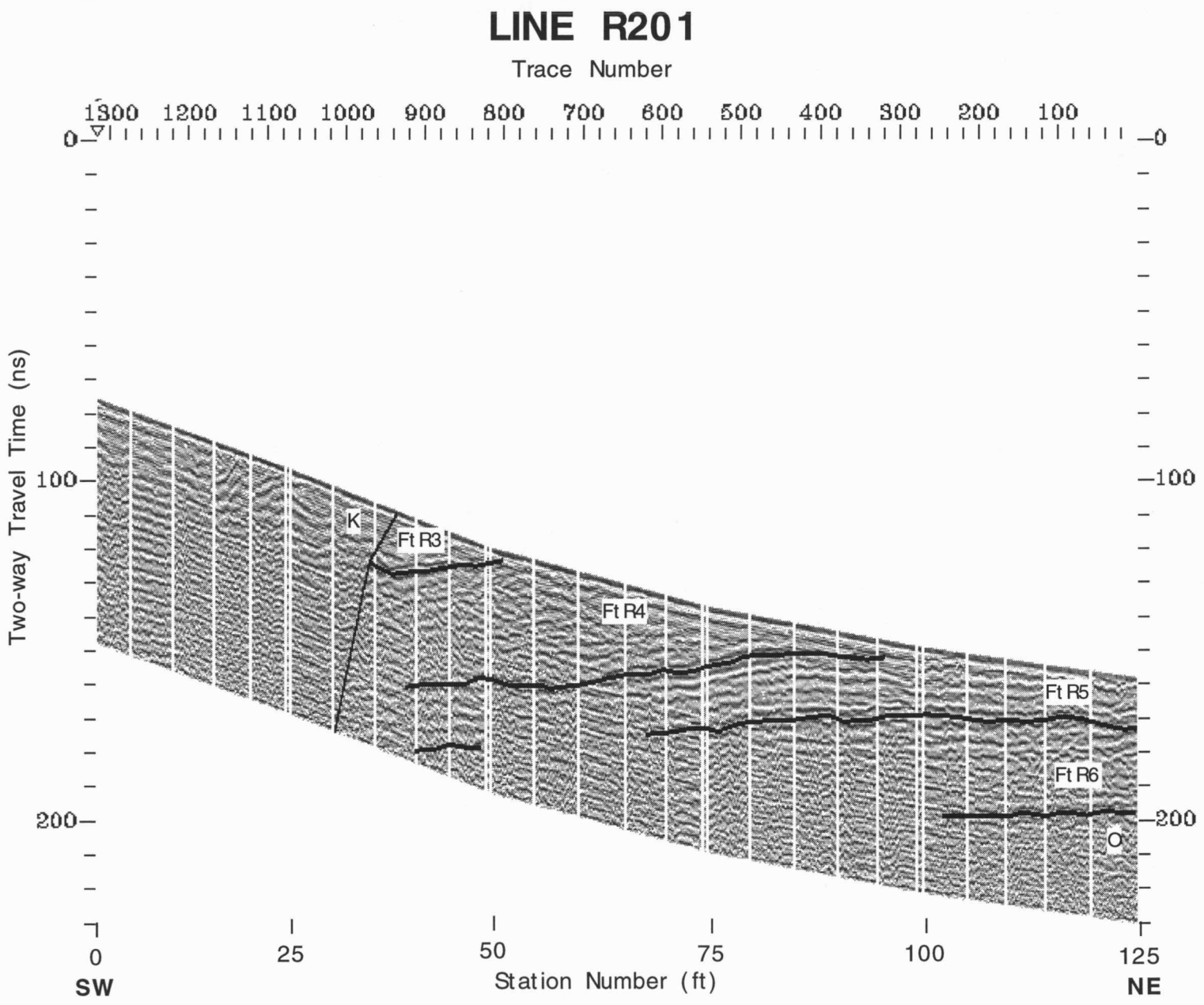
LINE R201
Trace Number
1300 1200 1100 1000 900 800 700 600 500 400 300 200 100
0
100
200
Two-way Travel Time (ns)
K
Ft R3
Ft R4
Ft R5
Ft R6
O
0
25
50
75
100
125
Station Number (ft)
SW
NE

Figure 15

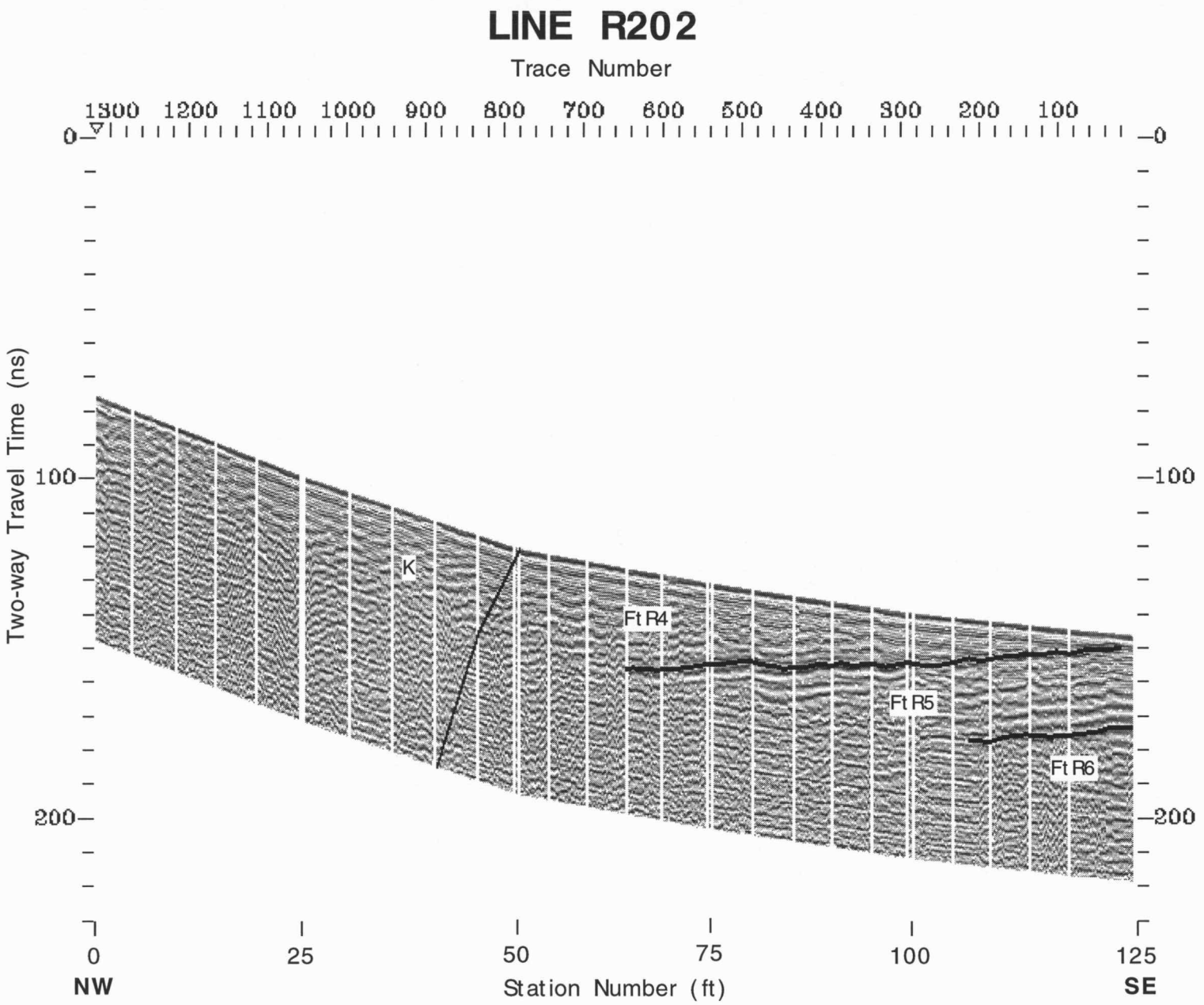
LINE R202
Trace Number
1300 1200 1100 1000 900 800 700 600 500 400 300 200 100
0
0
Two-way Travel Time (ns)
100
100
K
Ft R4
Ft R5
Ft R6
200
200
0
25
50
75
100
125
NW
Station Number (ft)
SE

Figure 16

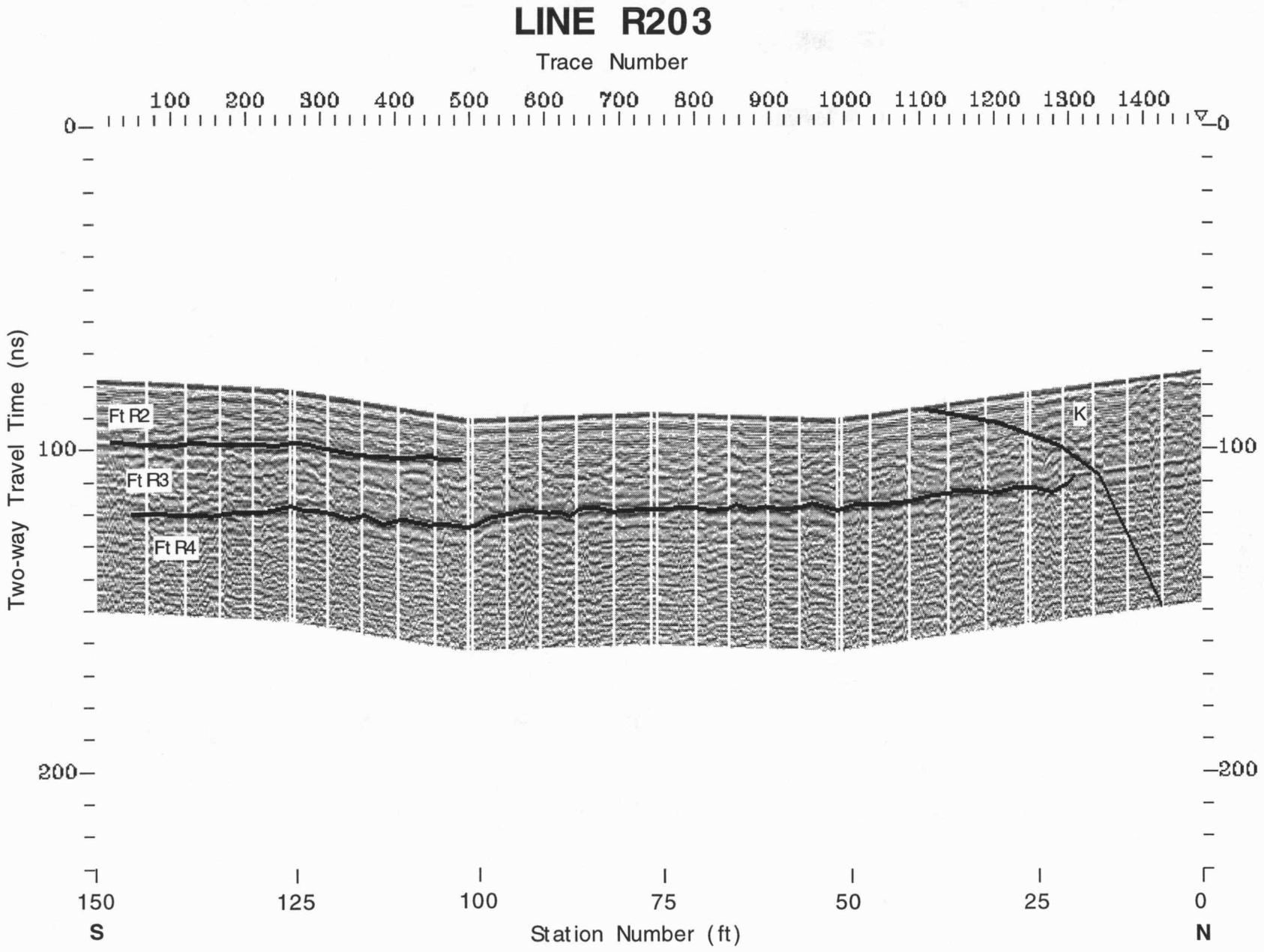
LINE R203
Trace Number
100 200 300 400 500 600 700 800 900 1000 1100 1200 1300 1400
0
Two-way Travel Time (ns)
100
200
Ft R2
Ft R3
Ft R4
K
150 125 100 75 50 25 0
S
Station Number (ft)
N

Figure 17

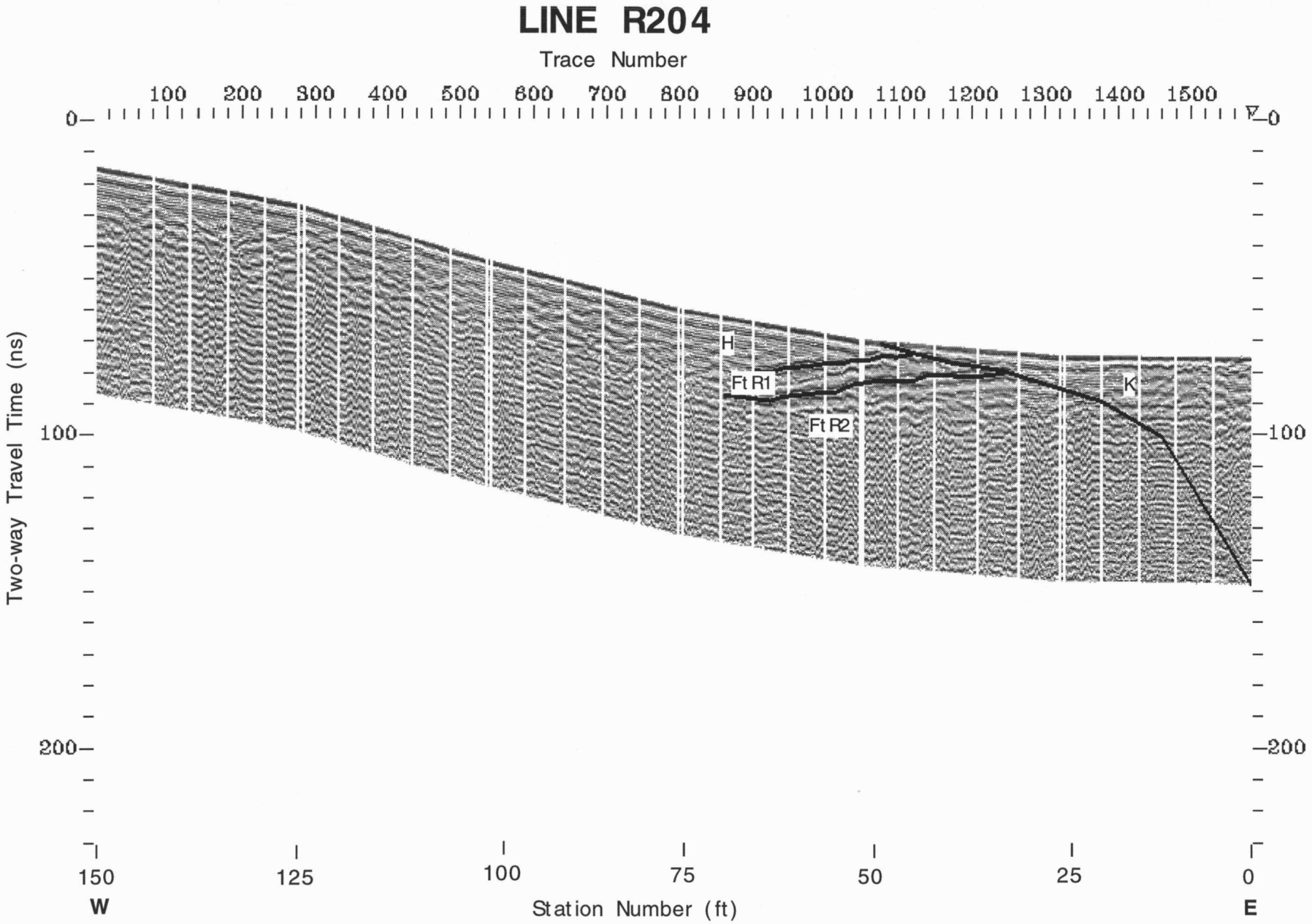
LINE R204
Trace Number
100
200
300
400
500
600
700
800
900
1000
1100
1200
1300
1400
1500
0
Two-way Travel Time (ns)
100
200
H
Ft R1
Ft R2
K
150
125
100
75
50
25
0
W
Station Number (ft)
E

Figure 18

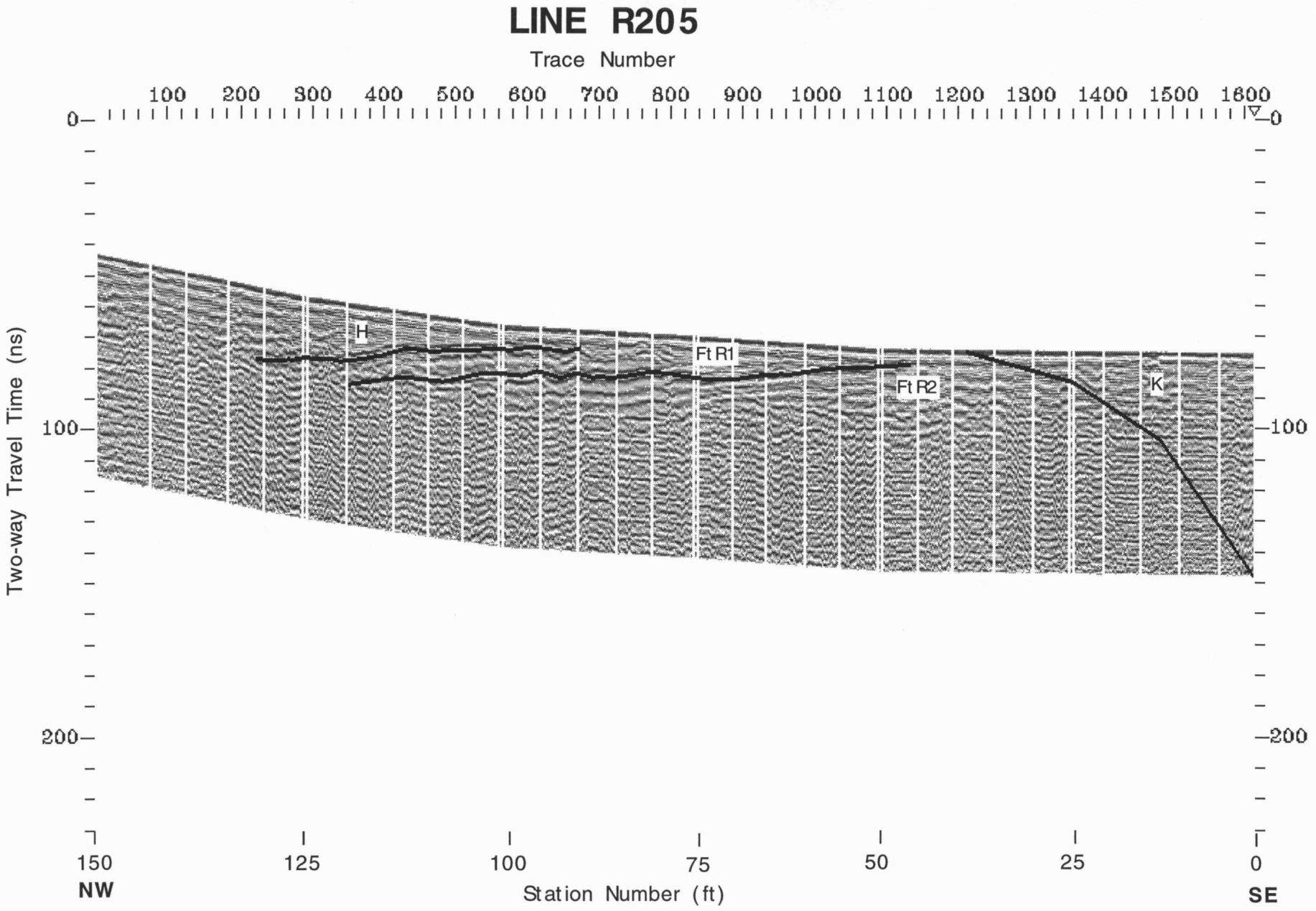
LINE R205
Trace Number
100 200 300 400 500 600 700 800 900 1000 1100 1200 1300 1400 1500 1600
0
100
200
Two-way Travel Time (ns)
H
Ft R1
Ft R2
K
150 125 100 75 50 25 0
NW
Station Number (ft)
SE

Figure 19

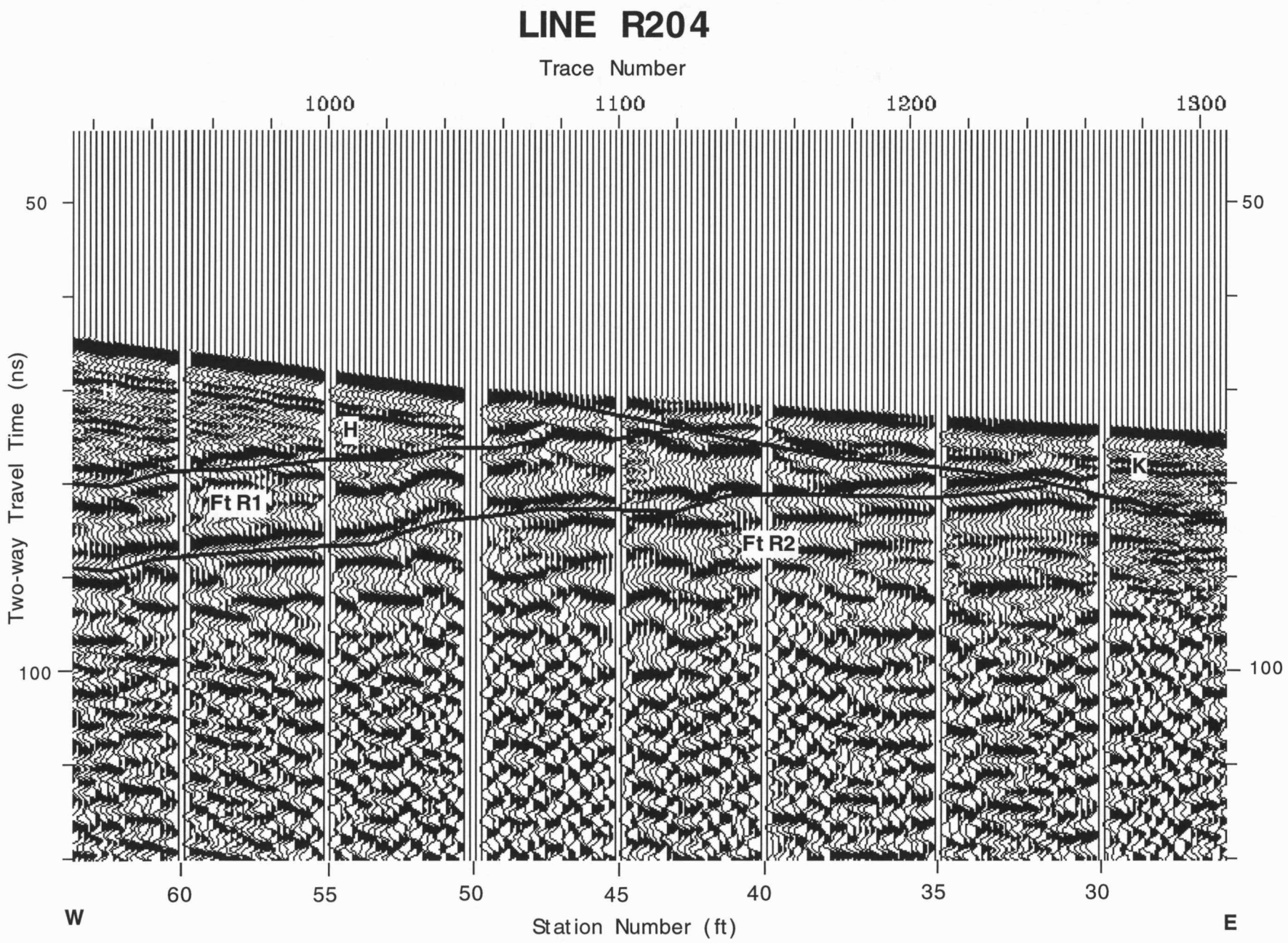
LINE R204
Trace Number
1000
1100
1200
1300
50
100
Two-way Travel Time (ns)
H
K
Ft R1
Ft R2
60
55
50
45
40
35
30
W
E
Station Number (ft)

Figure 20

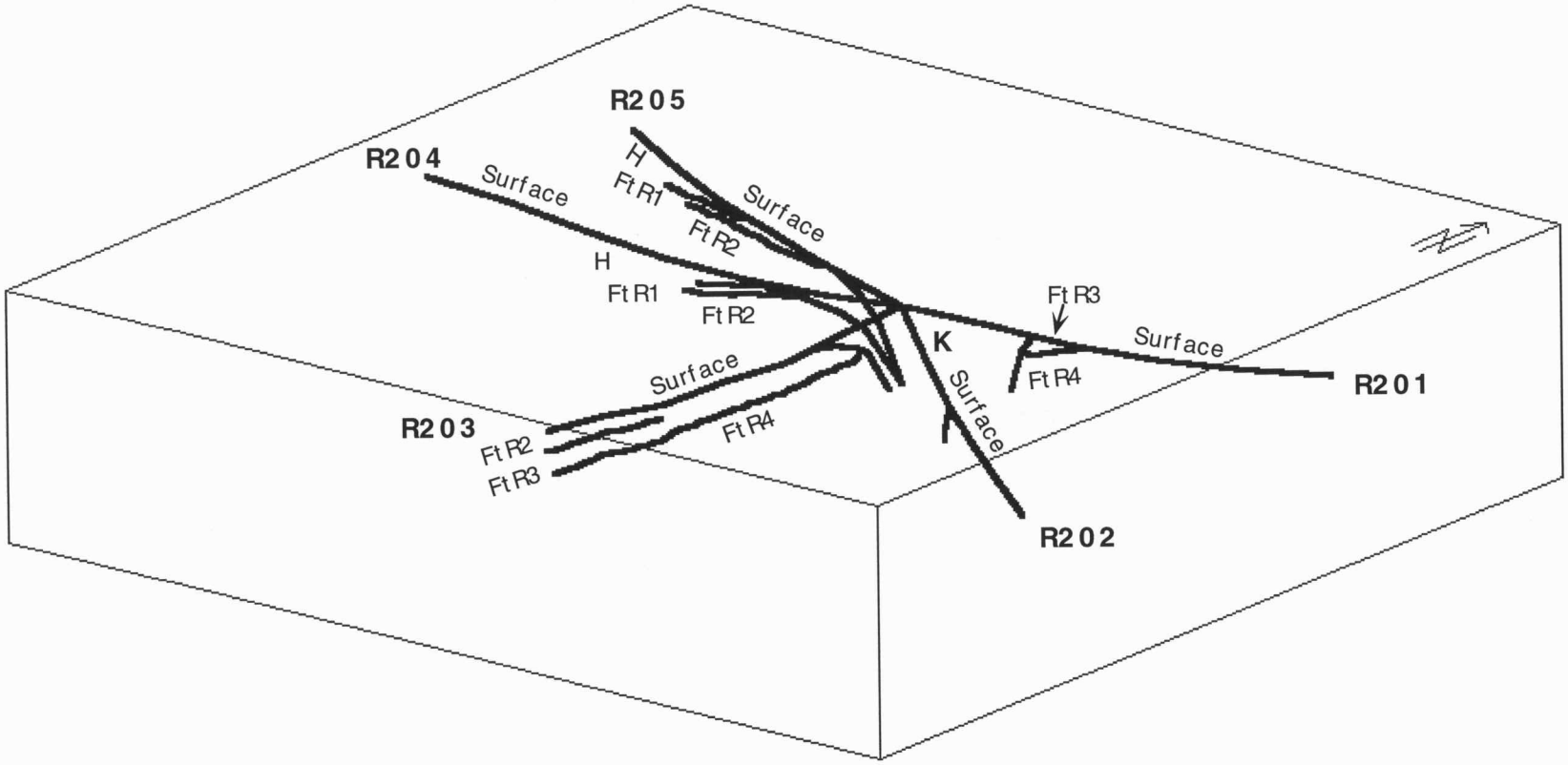
R205
R204
Surface
H
Ft R1
Ft R2
Surface
H
Ft R1
Ft R2
Ft R3
K
Surface
Surface
Ft R4
R201
Surface
R203
Ft R2
Ft R3
Ft R4
R202

Figure 21a

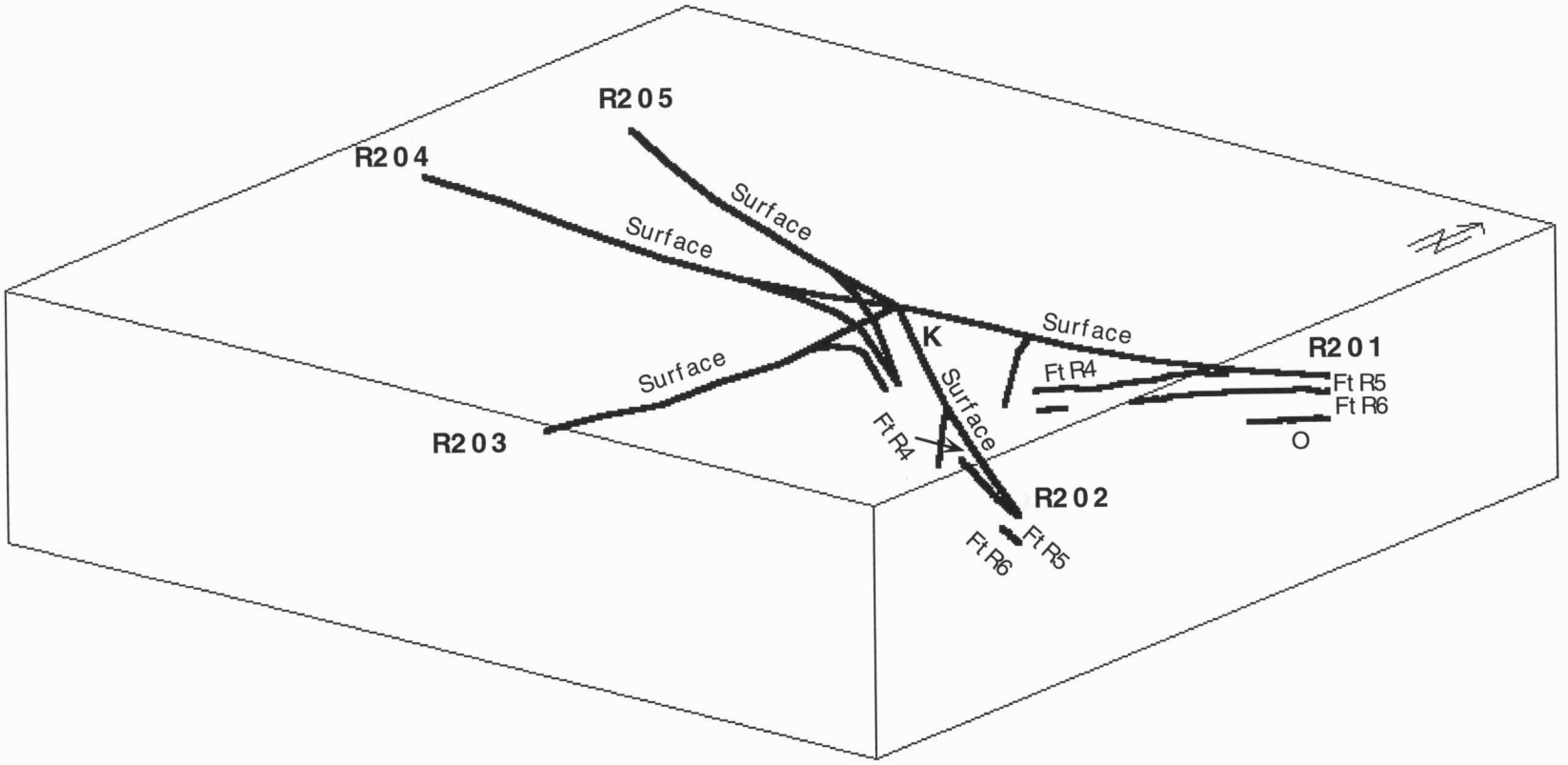
R205
R204
Surface
Surface
Surface
Surface
Surface
K
R201
Ft R4
Ft R5
Ft R6
O
R203
Ft R4
Surface
R202
Ft R6
Ft R5

Figure 21b

APPENDIX A: UNINTERPRETED DATA

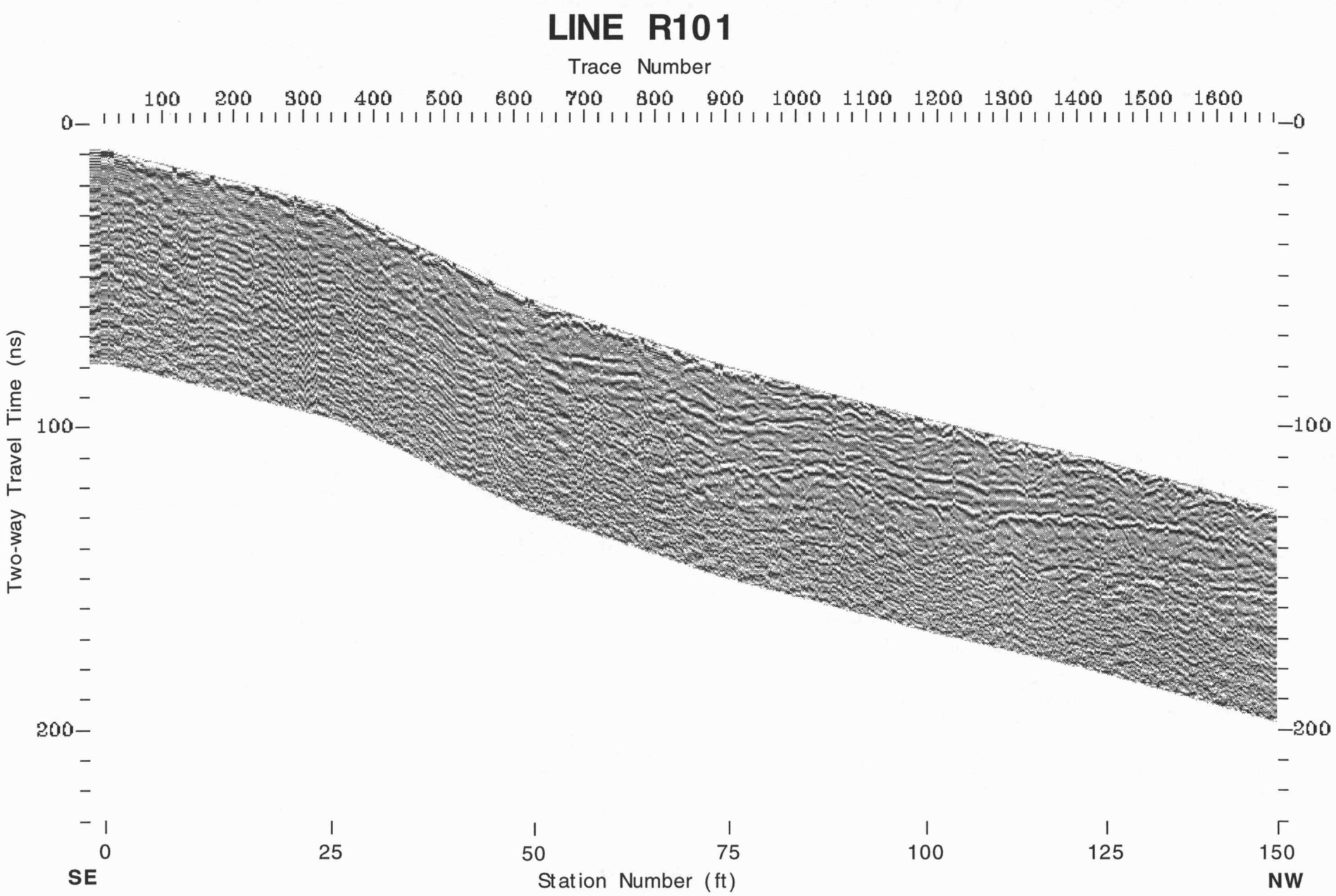
LINE R101
Trace Number
100 200 300 400 500 600 700 800 900 1000 1100 1200 1300 1400 1500 1600
0
100
200
Two-way Travel Time (ns)
0 25 50 75 100 125 150
Station Number (ft)
SE
NW

Figure 5

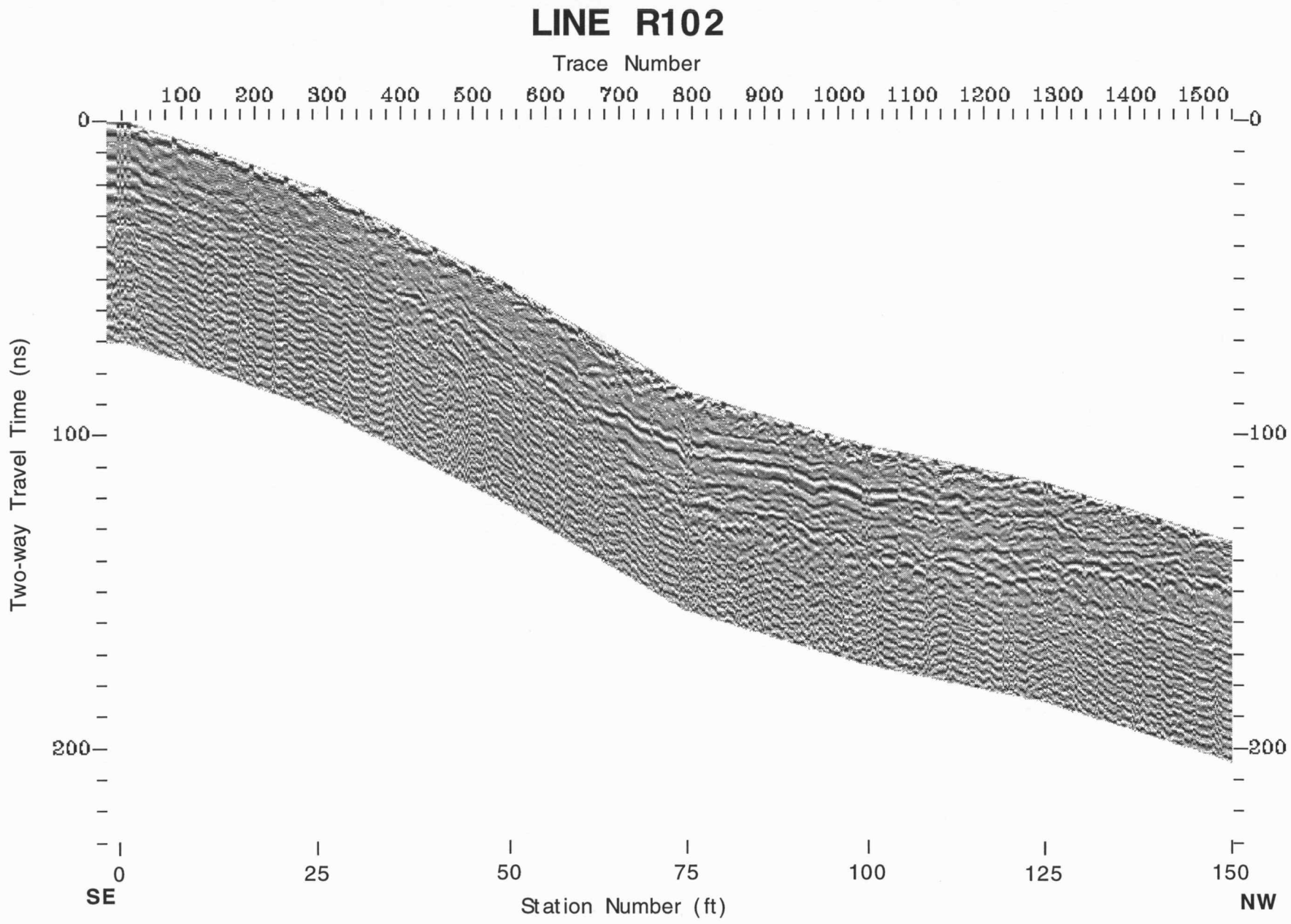
LINE R102
Trace Number
100 200 300 400 500 600 700 800 900 1000 1100 1200 1300 1400 1500
0
100
200
Two-way Travel Time (ns)
0 25 50 75 100 125 150
SE
NW
Station Number (ft)

Figure 6

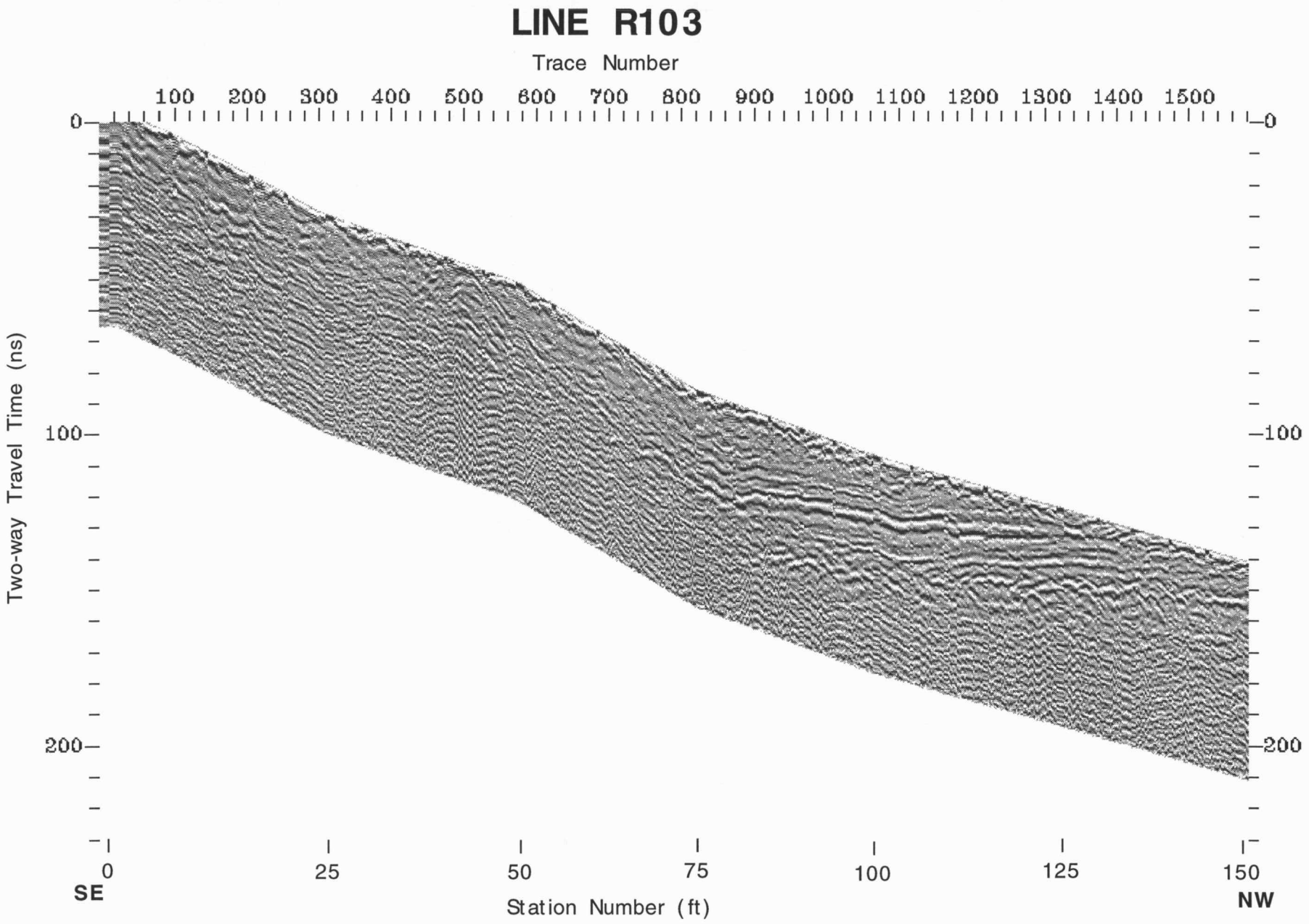
LINE R103
Trace Number
100 200 300 400 500 600 700 800 900 1000 1100 1200 1300 1400 1500
0
100
200
Two-way Travel Time (ns)
0 25 50 75 100 125 150
SE
NW
Station Number (ft)

Figure 7

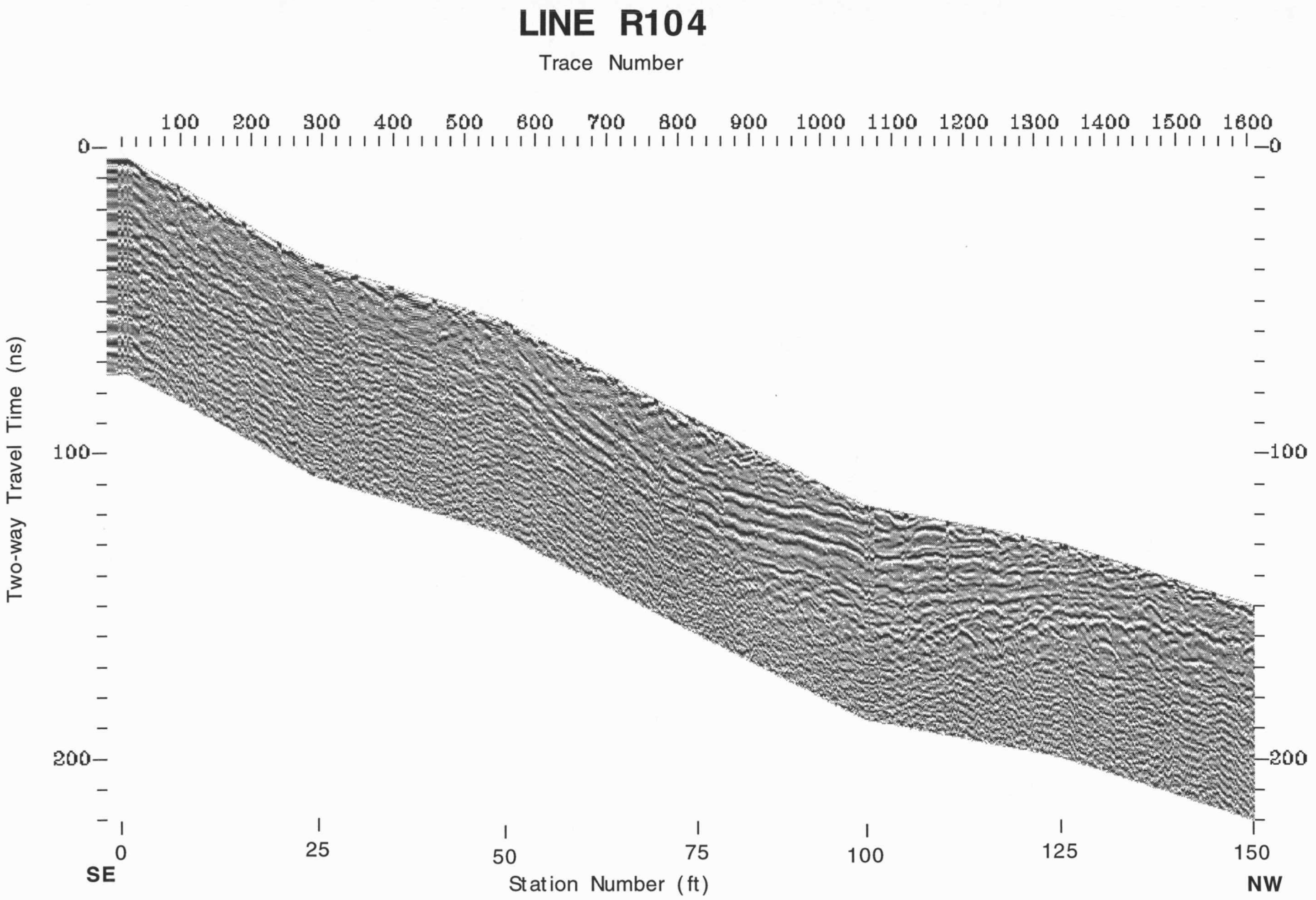
LINE R104
Trace Number
100 200 300 400 500 600 700 800 900 1000 1100 1200 1300 1400 1500 1600
0
100
200
Two-way Travel Time (ns)
0 25 50 75 100 125 150
SE
Station Number (ft)
NW

Figure 8

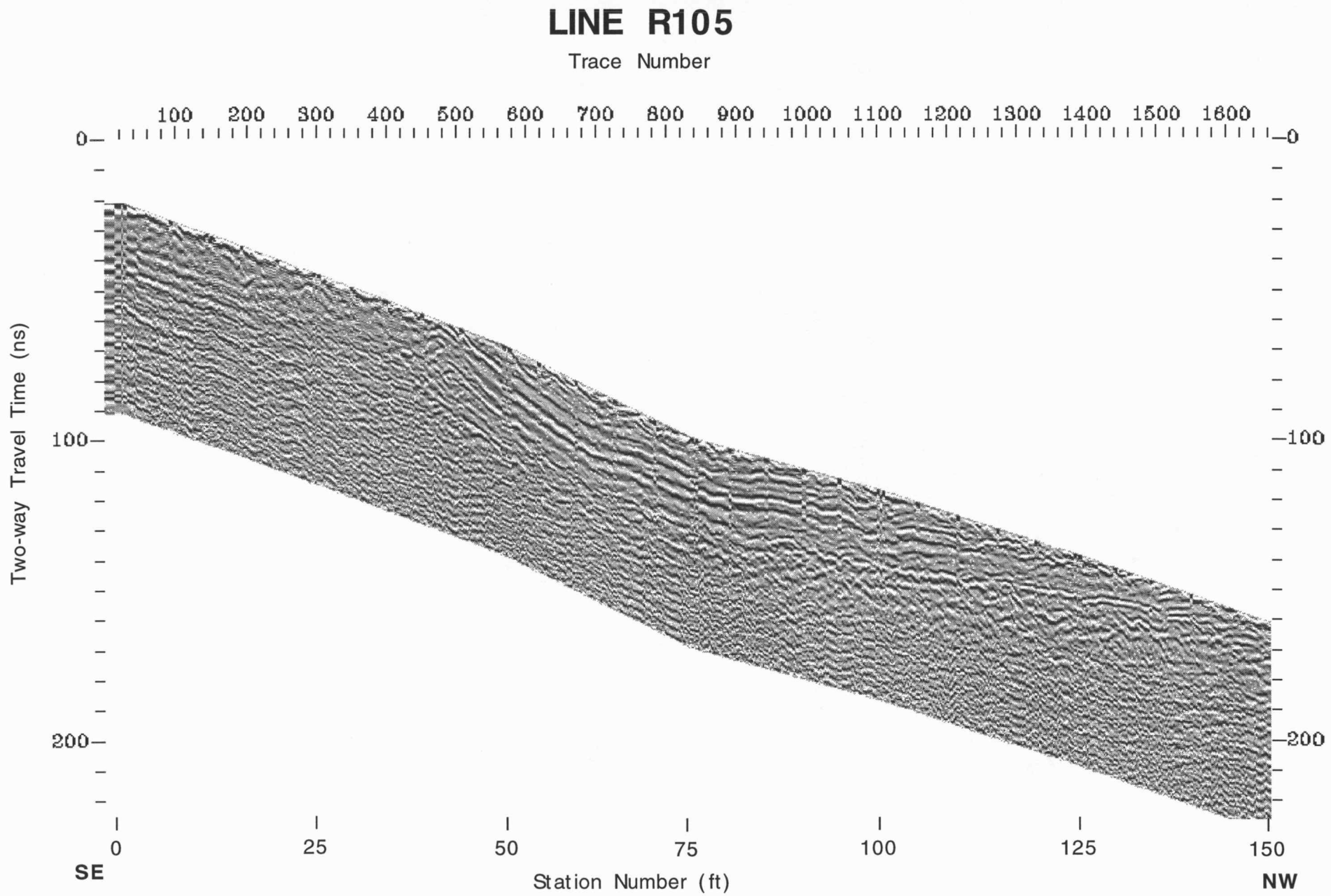
LINE R105
Trace Number
100 200 300 400 500 600 700 800 900 1000 1100 1200 1300 1400 1500 1600
0
100
200
Two-way Travel Time (ns)
0 25 50 75 100 125 150
SE
NW
Station Number (ft)

Figure 9

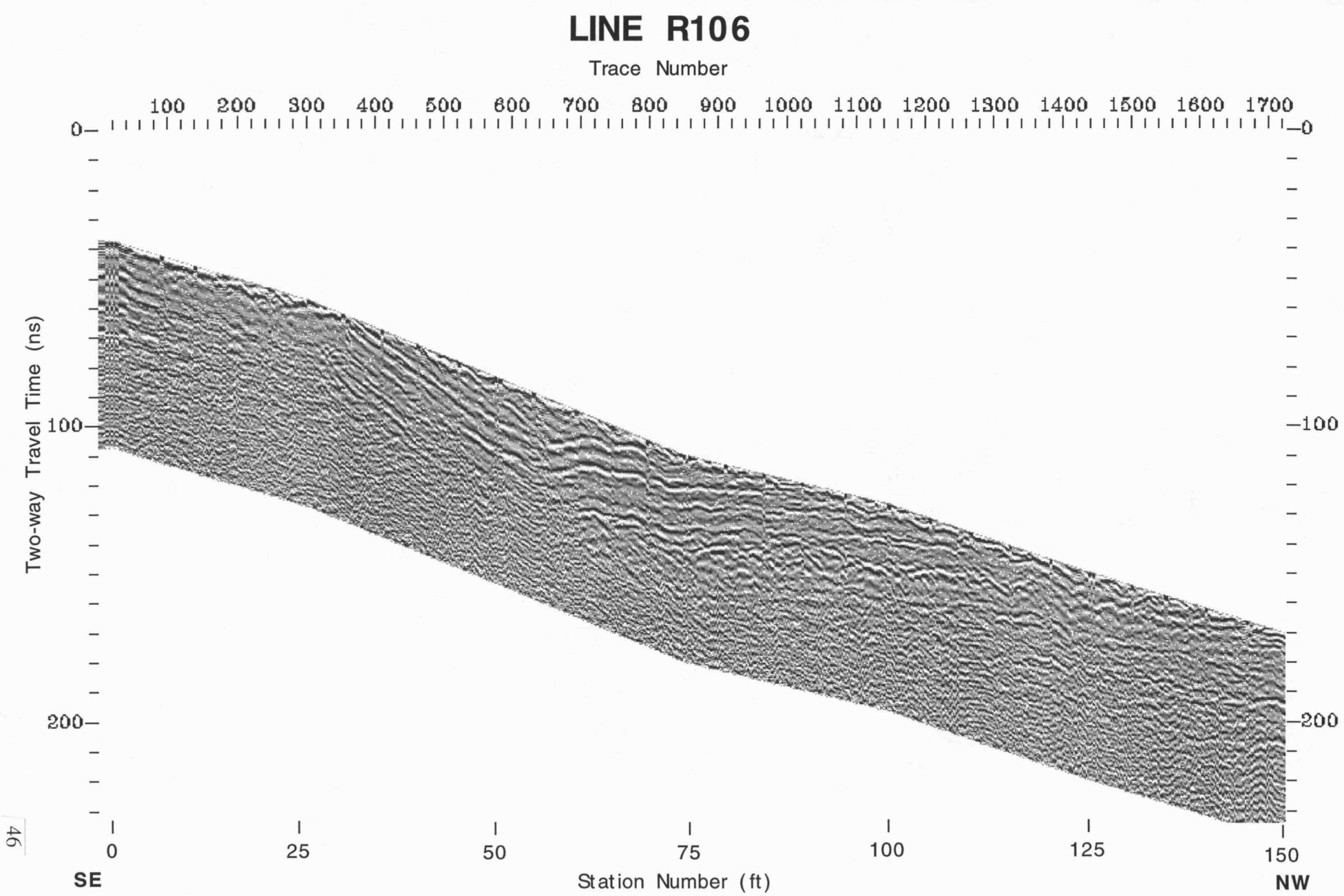
LINE R106
Trace Number
100 200 300 400 500 600 700 800 900 1000 1100 1200 1300 1400 1500 1600 1700
0
100
200
Two-way Travel Time (ns)
0 25 50 75 100 125 150
Station Number (ft)
SE
NW

Figure 10

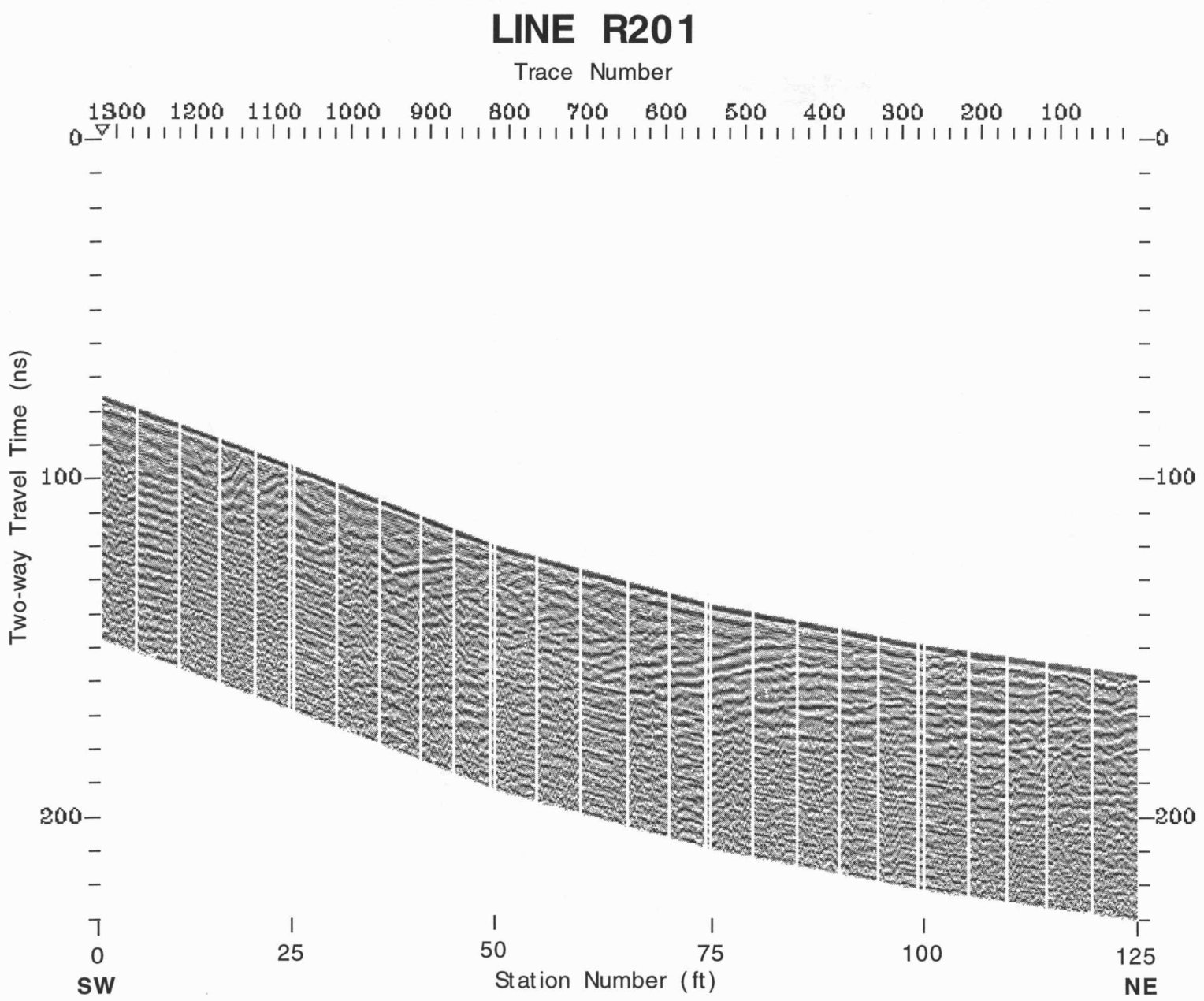
LINE R201
Trace Number
1300 1200 1100 1000 900 800 700 600 500 400 300 200 100
0
0
100
100
200
200
Two-way Travel Time (ns)
0
25
50
75
100
125
SW
Station Number (ft)
NE

Figure 15

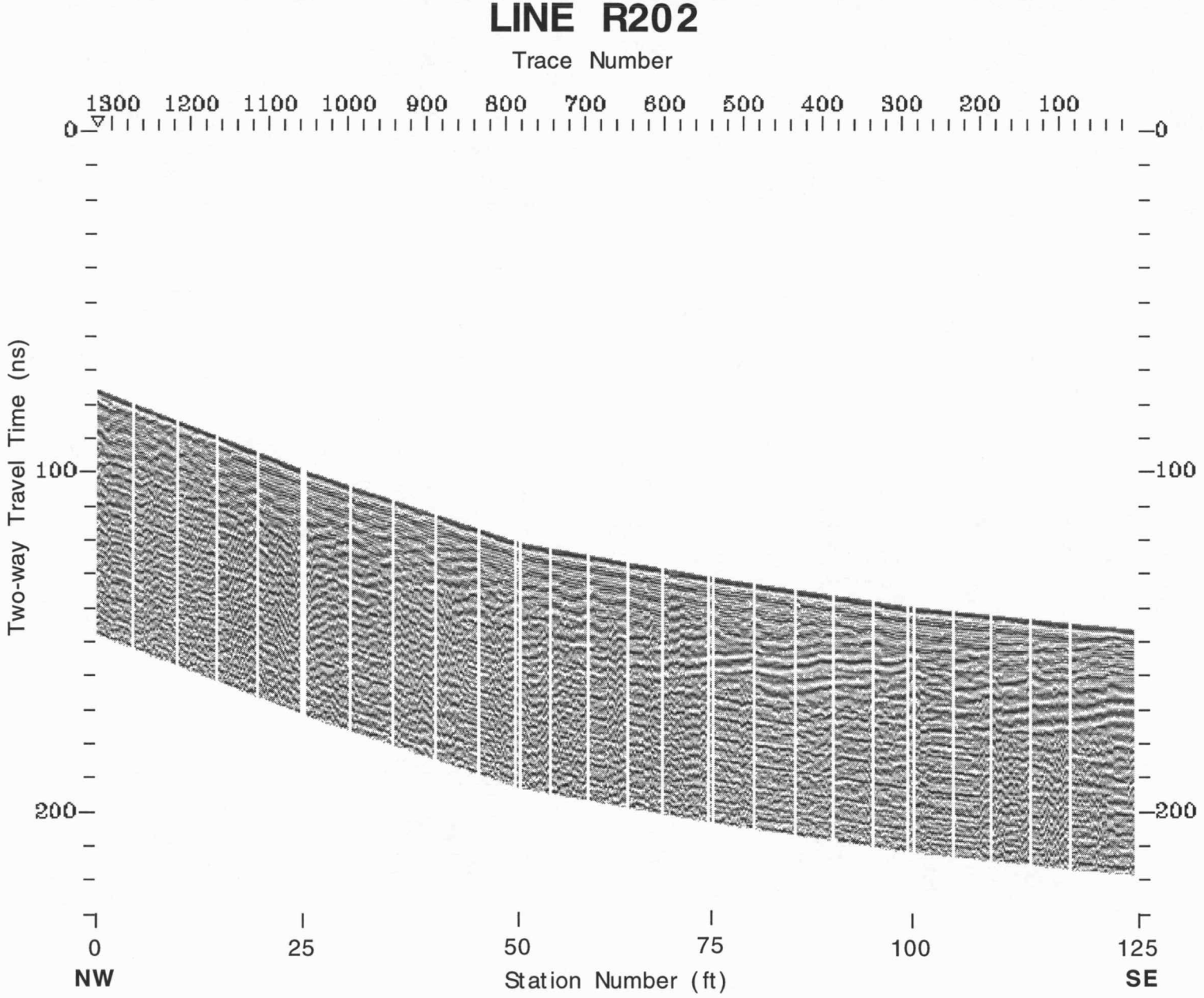
LINE R202
Trace Number
1300 1200 1100 1000 900 800 700 600 500 400 300 200 100
0
100
200
Two-way Travel Time (ns)
0 25 50 75 100 125
NW
Station Number (ft)
SE

Figure 16

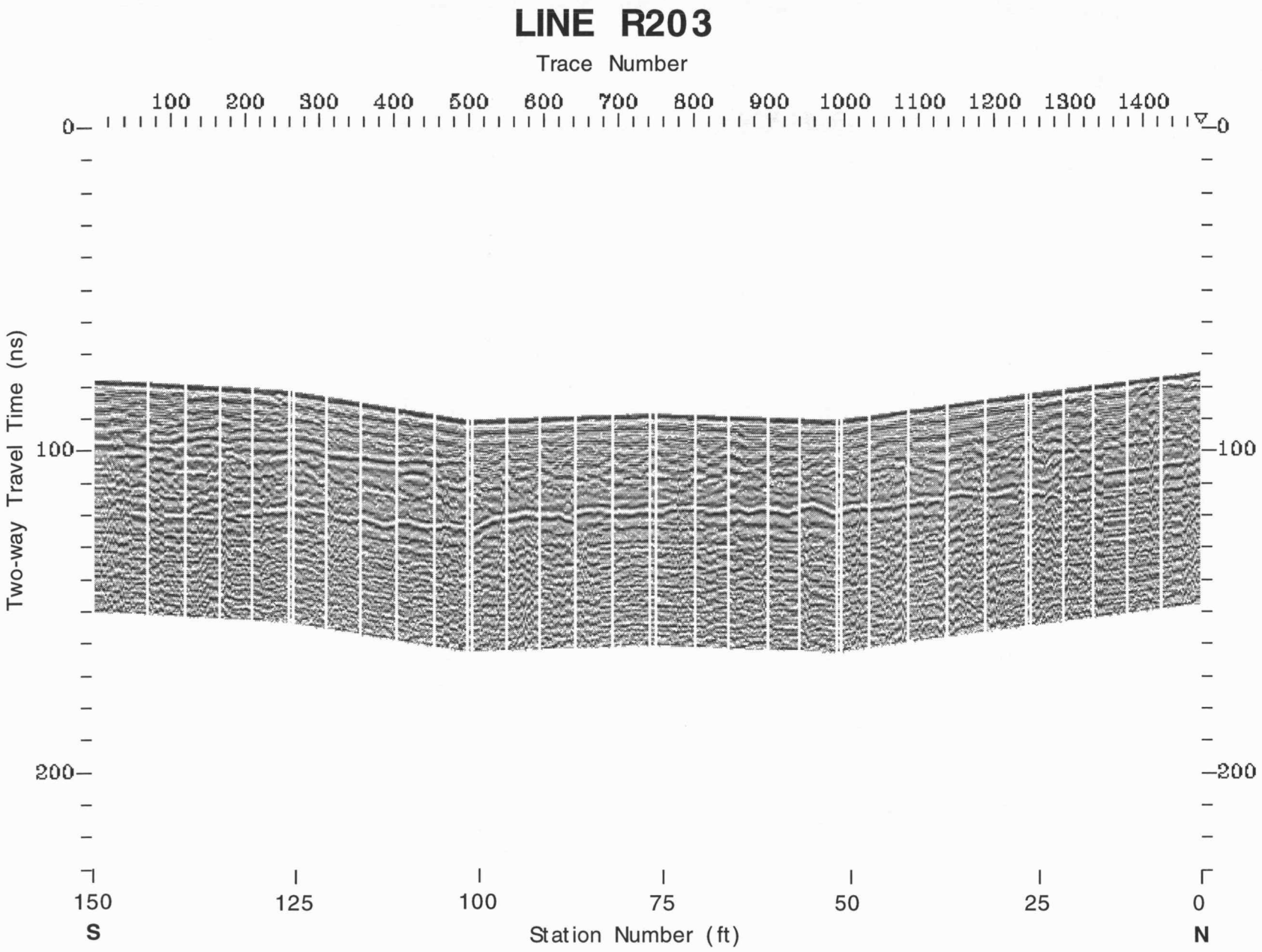
LINE R203
Trace Number
100 200 300 400 500 600 700 800 900 1000 1100 1200 1300 1400
0
Two-way Travel Time (ns)
100
200
150 125 100 75 50 25 0
S
Station Number (ft)
N

Figure 17

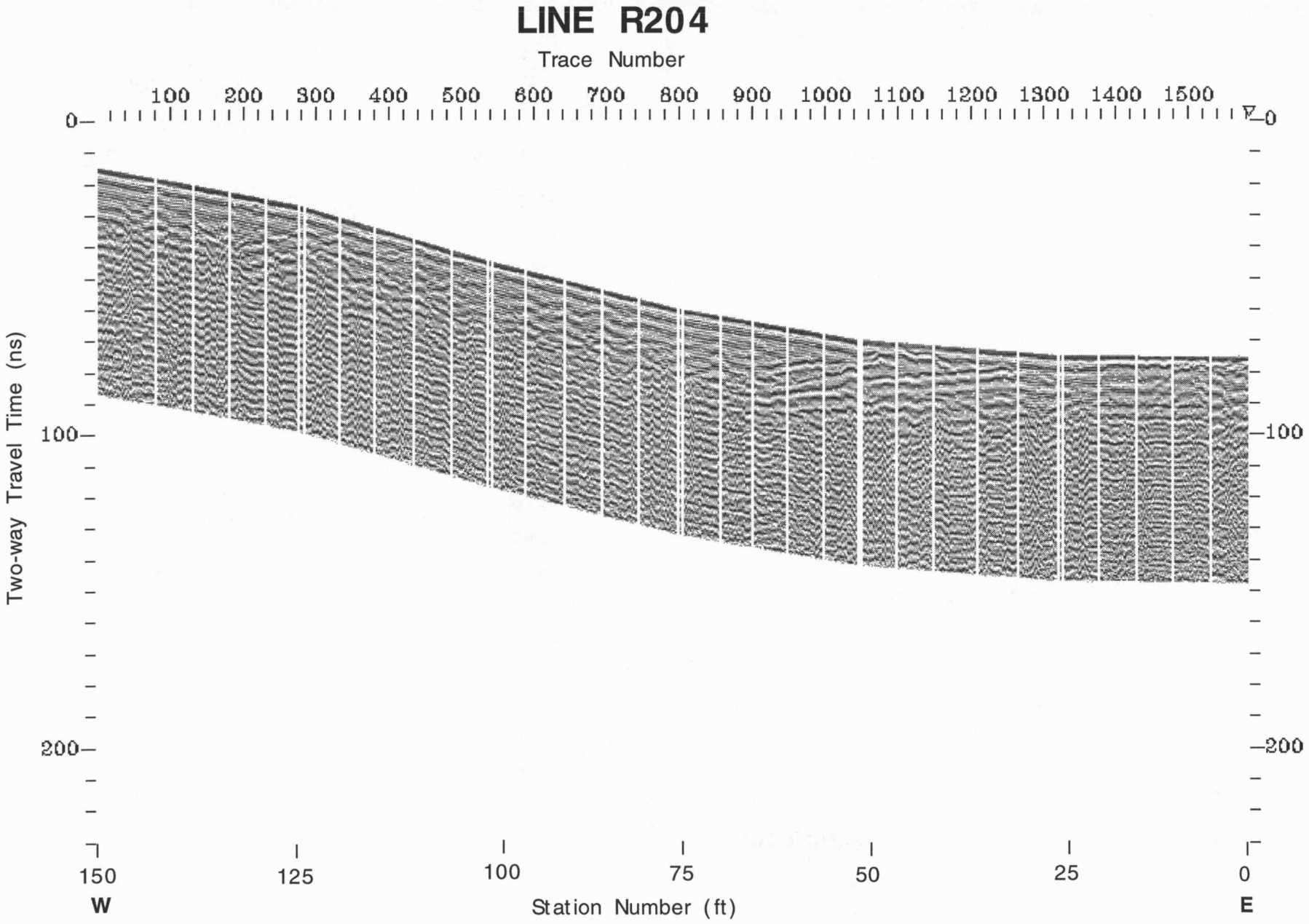
LINE R204
Trace Number
100 200 300 400 500 600 700 800 900 1000 1100 1200 1300 1400 1500
0
100
200
Two-way Travel Time (ns)
150
W
125
100
75
50
25
0
E
Station Number (ft)

Figure 18

LINE R205

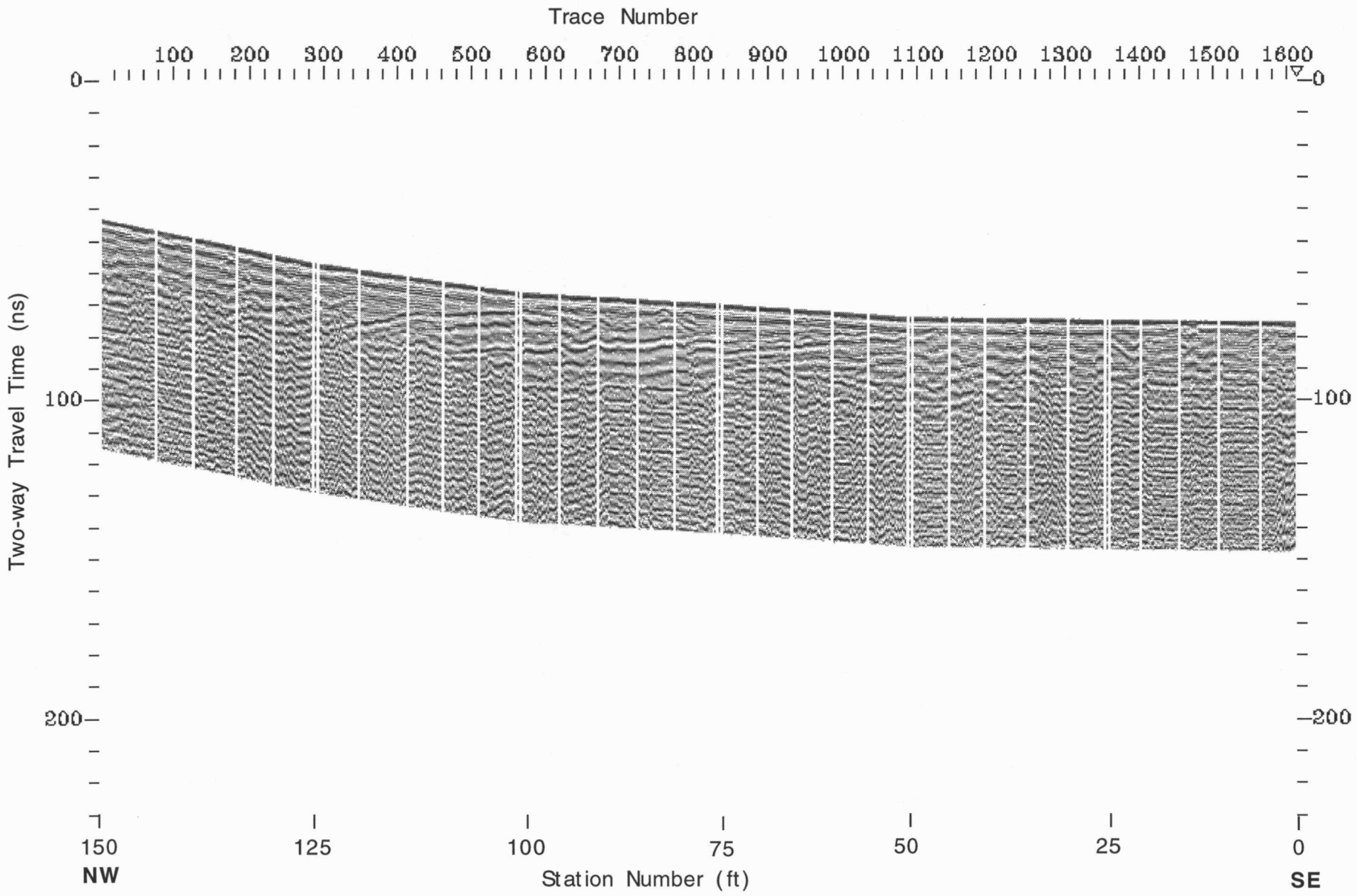

Figure 19